Appendix

Contents

Appendix A

A.1 Crystal data

Table 1 Selected bond lengths for PKH·3DMSO

Bond	Bond length (Å)
N2-C10	1.298(7)
N2-C11	1.383(7)
N1-C9	1.309(6)
N1-C12	1.367(7)
C10-C1	1.497(17)
C10-C9	1.430(7)
O2-C2	1.346(6)
O1-C1	1.239(6)
O3-C3	1.327(6)
C4-O4	1.224(6)
C4-C9	1.494(8)
C4-C3	1.473(7)
C1-C2	1.455(8)
C3-C2	1.342(7)

Table 2 Selected bond lengths for PKH·3DMSO

Bond	Bond angle (°)	Bond	Bond angle (°)
C10-N2-C11	116.4(5)	N1-C9-C4	119.6(5)
C9-N1-C12	116.0(4)	C10-C9-C4	113.8(4)
N2-C10-C1	118.0(5)	O3-C3-C4	122.2(5)
N2-C10-C9	122.8(5)	C2-C3-C4	120.9(8)
C9-C10-C1	119.2(5)	C6-C5-C12	123.6(7)
O4-C4-C9	120.2(5)	N2-C11-C12	120.4(5)
O4-C4-C3	121.2(5)	N2-C11-C8	120.9(5)
C3-C4-C9	118.5(5)	N1-C12-C5	120.2(5)
O1-C1-C10	120.6(5)	N1-C12-C11	121.5(5
O1-C1-C2	121.0(5)	O2-C2-C1	118.4(5)
C2-C1-C10	120.6(5)	C3-C2-O2	118.5(5)
N1-C9-C10	122.8(5)	C3-C2-C1	123.1(5)
C7-C8-C11	122.5(5)		
C8-C7-C6	118.7(5)		

Table 3 Selected bond lengths for PTK·CH_2Cl_2·2DMSO

Bond	Bond length (Å)	Bond	Bond length (Å)	Bond	Bond length (Å)
Cl1-C13	1.739(3)	O2-C2	1.380(3)	N1-C12	1.358(3)
Cl2-C13	1.758(3)	O6-C4	1.216(3)	O3-H3	0.8200
N2-C10	1.318(3)	O4-H4	0.8200	O3-C3	1.395(3)
N2-C11	1.364(3)	O4-C3	1.389(3)	O2-H2	0.8200
N1-C9	1.321(3)	O1-C1	1.213(3)		
O5-C2	1.402(3)	O5-H5	0.8200		

Table 4 Selected bond lengths for PTK·CH_2Cl_2·2DMSO

Bond	Bond angle (°)	Bond	Bond angle (°)
C10-N2-C11	116.9(2)	O4-C3-C4	108.57(18)
C9-N1-C12	116.8(2)	O4-C3-C2	111.80(18)
O1-C1-C10	121.6(2)	C4-C3-C2	108.6(2)
O1-C1-C2	122.4(2)	O6-C4-C3	123.5(2)
C10-C1-C2	115.98(19)	O6-C4-C9	121.3(2)
O3-C3-C4	108.02(18)	N1-C9-C4	117.3(2)
O3-C3-C2	105.41(17)	N1-C9-C10	122.0(2)
O4-C3-O3	114.2(2)	N2-C10-C1	117.7(2)
O5-C2-C3	110.29(18)	N2-C10-C9	122.3(2)
C1-C2-C3	108.54(18)	O2-C2-O5	114.30(18)
N2-C11-C8	120.0(2)	O2-C2-C1	112.90(19)
N2-C11-C12	120.7(2)	O2-C2-C3	107.2(2)
N1-C12-C5	120.0(2)	O5-C2-C1	103.5(2)
N1-C12-C11	121.3(2)		

Table 5 Selected bond lengths for HATN-4Me·2$CHCl_3$

Bond	Bond length (Å)	Bond	Bond length (Å)	Bond	Bond length (Å)
N3-C16	1.352(7)	C24-N6	1.338(7)	N6-C17	1.323(7)
N3-C21	1.300(7)	C20-N2	1.317(6)	C13-N2	1.363(7)
C15-N4	1.337(8)	C23-N5	1.324(7)	C14-N1	1.316(7)
C22-N4	1.356(7)	N5-C18	1.331(8)	C19-N1	1.347(7)

Table 6 Selected bond angles for HATN-4Me·2CHCl$_3$

Bond angle (°)	Bond angle (°)	Bond angle (°)	Bond angle (°)
C21-N3-C16	117.3(4)	N6-C17-C18	121.7(5)
N4-C15-C16	122.5(4)	N2-C13-C14	120.6(5)
N4-C15-C8	118.4(5)	N2-C13-C4	120.4(6)
N4-C22-C23	119.3(5)	N5-C18-C17	122.4(5)
N4-C22-C21	119.9(5)	N5-C18-C9	118.5(5)
N6-C24-C23	121.3(5)	N3-C21-C22	122.7(4)
N6-C24-C19	117.6(4)	N3-C21-C20	118.5(4)
N2-C20-C19	121.5(5)	N1-C14-C1	119.0(5)
N2-C20-C21	118.2(5)	N1-C19-C24	118.7(5)
N5-C23-C22	118.5(4)	N1-C19-C20	121.8(5)
N5-C23-C24	122.1(5)	C17-N6-C24	116.4(4)
C15-N4-C22	116.5(5)	N3-C16-C15	121.0(5)
C23-N5-C18	115.9(4)	N3-C16-C5	120.6(5)
N1-C14-C13	121.8(4)	N6-C17-C12	118.5(5)

Appendix B

B.1 UV/Visible spectroscopy

Solution UV-Visible absorbance spectra were recorded on a Shimadzu UV-3101PC UV-VIS-NIR-scanning spectrophotometer. Samples were recorded in chloroform at concentrations near 10^{-6} M.

B.2 Vibrational spectroscopy

All ground state vibrational measurements were taken in the solid state on a Nicolet 5700 FT-IR from Thermo Electron Corporation using an ATR attachment. Continuous wave excitation was used for all Raman measurements. Raman spectroscopy was carried out on the Bruker Equinox 55 interferometer equipped with the Bruker FRA 106/S FT-Raman accessory, with the source Nd:YAG laser at 1064 nm. The defocused aperture setting that gave a 1 mm diameter spot size was used, with a power setting of 120 mW and a resolution of 4 cm^{-1}.120 scans were co-added to produce a spectrum with an acceptable signal/noise ratio.

B.3 Dye Adsorption

All plates were pre-prepared by Dr. Wayne Campbell. Using a cutting guide the TiO_2 plates were prepared by cutting 10 x 15 mm sections of the TiO_2 coated glass. The TiO_2 surface was placed face down on lint-free tissue paper, taking care not to damage the surface during cutting. Cutting with a standard glasscutter was found easier using hexane inside the glass cutter. One edge of the TiO_2 layer was then scraped back for an electrode contact point, leaving about 10 x 10 mm TiO_2 square, with the TiO_2 extending fully to 3 edges. The TiO_2 plates were then then pre-treated by washing with ethanol (30 min), hexane (30 min), Milli Q water (30 min) and then rinsed with ethanol prior to drying and firing at 480 $^{\circ}C$ for 30 min. All TiO_2 plates were carefully handled with tweezers and powder-free gloves to avoid contamination.

Prior to dye adsorption, the plates were fired again at 480 °C for 0.5 h and then immersed in the dye solution while still warm. The plates were immersed in a sealed container of dye solution (10^{-4} M) for over-night adsorption (12-20 hours) prior to testing. The TiO_2 plates were removed from the dye solution directly before testing and the excess solvent removed by blotting on lint-free tissue paper. These dyed plates were then dried under high vacuum for 5 minutes prior to cell assembly in cell holder.

B.3.1 Electrolytes (DSSC)

The electrodes were polished before use. Several dyes were tested but only two were consistently used in this study, E-Zn3 and E-Th1, there details are given in Table 7.

Table 7 DSSC electrolytes

Electrolyte	Composition
E-Zn	0.1 M LiI, 0.05 M I_2, 0.5 M 4-tert-butylpyridine, 0.6M BMII[a], 0.5 M BHT[b] in 1:1 valeronitrile:glutaronitrile
E-Th	0.1 M LiI, 0.05 M I_2, 0.6 M BMII in glutaronitrile

[a] 1-butyl-3-methylimidazolium iodide

[b] Butylated hydroxytoluene

B.4 Field Effect Transistor Device fabrication

300 nm SiO_2 on Si was cut to size and washed with acetone and methanol in a sonicator and dried with air. The surface was then cleaned with the Plasma Etch using O_2. A 20 s O_2 plasma treatment helps give a cleaner substrate which results in better material adhesion.

Once the surface was ready, 100 μL HATN was spin-coated for 1 minute (2500 rpm) using $CHCl_3$ as the solvent. The chips were then annealed at 145 $^{\circ}$C for 10 minutes, or left in ambient conditions (stated in work).

The Si Chips were put into a mask where the channels were mapped out by using a AZ 1518 resist. The Angstrom engineering evaporator had an INFICON rate deposition controller with rotating substrate holder which enabled the creation of very accurate gold film thicknesses on the surface. The gate and source electrodes were made to be 45 nm thick.

The Agilent 4156C (Precision Semiconductor Parameter Analyser) was connected to the probe station and came equipped with four high-resolution source measure units (SMUs). The probe station was set up with four high precision Ti probes on micromanipulators and was housed in a custom-made Faraday box with a high quality co-axial cable running to the micromanipulator. The probe station was equipped with a vacuum chuck and objective lenses of various magnification for maximum flexibility. The source, drain and gate are connected to the device which was then ready for measurement.

B.5 Electrochemistry methods

Solution state (staircase) cyclic voltammetry (CV) measurements were performed using a three electrode system comprised of a macro platinum working electrode, a macro platinum auxiliary (counter) electrode and a silver/silver chloride (Ag/AgCl) reference electrode. CV measurements were performed on 0.5 $x10^{-4}$ mM solutions using 0.1 M tetra-*n*-butylammonium bromide (TBABr) as the supporting electrolyte. A reference CV of ferrocene in 0.1 M TBABr was acquired. Using literature values for the ferrocene redox couple with respect to a Ag/AgCl reference electrode all potential values are reported with respect to a Fc/Fc+ reference electrode.[2,3]

Literature values reported with respect to reference electrodes other than a Fc/Fc+ electrode (i.e the normal hydrogen electrode (NHE)) have been converted to be with respect to a Fc/Fc+ electrode to make comparisons with the potential values in this thesis. This conversion was achieved using literature values for the NHE electrodes.

To calculate electronic bandgaps for each molecule the HOMO potential was calculated from the cyclic voltammograms (with respect to Fc/Fc+). To convert the Eonsetox values into a HOMO potential, the following relationship was used:[4]

Ionisation Potential (HOMO) = Eonsetox (vs Fc/Fc+) + 4.4 eV

The bandgap was estimated from onset wavelength (λonset) of the lowest energy band in the absorption spectra. To calculate the bandgap, the UV-Vis onset wavelength was converted to energy (in eV) using Planck's equation E = hυ (where 1243 is the conversion factor to energy in eV):

$$\text{Band gap (eV)} = \frac{1243}{\lambda_{onset}(nm)}$$

This allowed a retrospective calculation of the LUMO potential of each compound.

B.6 MAD Values

Table 8 MAD Value between crystal data and calculated data for HATN-4Me

Bond	Calculated Value (Å)	Crystal Value (Å)	Difference
N3-C16	1.351	1.352	0.001
N4-C15	1.351	1.337	0.014
N3-C21	1.326	1.300	0.026
N4-C22	1.326	1.356	0.030
N2-C20	1.326	1.317	0.009
N1-C19	1.326	1.347	0.021
N2-C15	1.351	1.363	0.012
N1-C14	1.351	1.316	0.035
N5-C23	1.324	1.324	0.000
N6-C24	1.324	1.338	0.014
N5-C18	1.353	1.331	0.022
N6-C17	1.353	1.323	0.030
MAD Value			0.018

Table 9 Mean difference in vibrational modes between IR and Raman data and DFT models.

HATN	Raman	IR	Average
HATN-4Me	1.7	10.1	5.9
HATN-4Br	16.5	14.3	15.4
HATN-2Me	7.6	12.4	10.0
HATN-4Br2Me	14.0	13.8	13.9
HATN-2Br	20.0	14.0	17.0
HATN-4Me2Br	8.8	11.9	10.4
Average	12.2	12.8	12.5

B.7 Excitation Tables of HATNs

Excitation table of the various HATNs were put together of excitations that had a oscillator strength higher than 0.001 otherwise they were ignored. TD-DFT calculations were carried out in a chloroform solvent field using the SCRF-PCM method which creates the solvent cavity via a set of overlapping spheres.

Table 10 First 10 excitations of HATN-4Me

λ	E	*f*	Transition	Coefficients	Major Contributors	Assignment
395.38	3.1358	0.1179	HOMO-2 →LUMO+2 HOMO → LUMO	0.11	π→π* π→π* π→π*	π→π*
389.50	3.1831	0.1318	HOMO-1 → LUMO	0.67		π→π*
378.68	3.2741	0.0055	HOMO-5 → LUMO HOMO-4 → LUMO HOMO-4 → LUMO+1 HOMO-3 → LUMO+2	0.67	n→π* n→π* n→π* n→π*	n→π*
376.94	3.2892	0.0071	HOMO-2 → LUMO HOMO-1 → LUMO+2 HOMO → LUMO+1	0.58	π→π* π→π* π→π*	π→π*
355.93	3.4834	0.0290	HOMO-2 → LUMO HOMO-1 → LUMO+2 HOMO → LUMO+1	-0.13	π→π* π→π* π→π*	π→π*
339.37	3.6534	0.0272	HOMO-7 → LUMO HOMO-2 → LUMO+2 HOMO-1 → LUMO+1 HOMO → LUMO+2	0.22	π→π* π→π* π→π* π→π*	π→π*

Continued excitations of **HATN-4Me**

λ	E	*f*	Transition	Coefficients	Major Contributors	Assignment
337.91	3.6692	0.0303	HOMO-6 → LUMO	-0.25	π→π*	π→π*
			HOMO-2 → LUMO+1		π→π*	
			HOMO → LUMO+1		π→π*	
331.36	3.7416	0.4745	HOMO-7 → LUMO	0.63	π→π*	π→π*
			HOMO-2 → LUMO+2		π→π*	
			HOMO-1 → LUMO+1		π→π*	
			HOMO → LUMO+2		π→π*	
331.32	3.7421	0.7931	HOMO-6 → LUMO	-0.15	π→π*	π→π*
			HOMO-2 → LUMO+1		π→π*	
			HOMO-1 → LUMO+2		π→π*	
			HOMO → LUMO+1		π→π*	
			HOMO-3 → LUMO+2		n→π*	
317.48	3.9052	0.7761	HOMO-6 → LUMO	-0.21	π→π*	π→π*
			HOMO-2 → LUMO+1		π→π*	
			HOMO-1 → LUMO+2		π→π*	
			HOMO → LUMO+1		π→π*	

Table 11 First 10 excitations of HATN-4Br

λ	E	*f*	Transition	Coefficients	Major Contributors	Assignment
406.18	3.0524	0.2952	HOMO →LUMO	0.68	π→π*	π→π*
401.07	3.0913	0.0898	HOMO-2 → LUMO+1 HOMO-1 → LUMO	0.12	π→π* π→π*	π→π*
385.51	3.2161	0.0051	HOMO-7→ LUMO HOMO-5→ LUMO+1 HOMO-3→ LUMO HOMO-3→ LUMO+2	0.67	π→π* π→π* π→π* π→π*	π→π*
385.12	3.2194	0.0462	HOMO-2 → LUMO HOMO-1→ LUMO+1 HOMO → LUMO+2	0.60	π→π* π→π* π→π*	π→π*
371.10	3.3409	0.0156	HOMO-1→ LUMO+2 HOMO → LUMO+1	-0.25	π→π* π→π*	π→π*
360.54	3.4388	0.0533	HOMO-2→ LUMO HOMO-1→ LUMO+1 HOMO → LUMO+2	0.10	π→π* π→π* π→π*	π→π*

Continued excitations of **HATN-4Br**

λ	E	*f*	Transition	Coefficients	Major Contributors	Assignment
348.03	3.5624	0.0704	HOMO-4 → LUMO HOMO-2→ LUMO+2 HOMO-1→ LUMO+1	0.17	π→π* π→π* π→π*	π→π*
346.74	3.5758	0.0167	HOMO-4 → LUMO HOMO-1→ LUMO+1 HOMO → LUMO+2	0.65	π→π* π→π* π→π* π→π*	π→π*
340.52	3.6410	0.5205	HOMO-6→ LUMO HOMO-2→ LUMO+1	-0.15	π→π* π→π*	π→π*
335.52	3.6952	0.4966	HOMO-6→ LUMO HOMO-2→ LUMO+1 HOMO-1→ LUMO+2 HOMO → LUMO+1	-0.12	π→π* π→π* π→π* π→π*	π→π*

Table 12 First 10 excitations of HATN-2Me

λ	E	*f*	Transition	Coefficients	Major Contributors	Assignment
390.28	3.1768	0.1173	HOMO-2 →LUMO+1 HOMO →LUMO	-0.11	π→π* π→π*	π→π*
388.66	3.1901	0.0889	HOMO-1 → LUMO	0.67	π→π*	π→π*
380.53	3.2582	0.0056	HOMO-5 → LUMO HOMO-4 → LUMO+1 HOMO-3 → LUMO HOMO-3 → LUMO+2	0.67	π→π* n→π* n→π* n→π*	n→π*
372.72	3.3265	0.0163	HOMO-2 → LUMO HOMO-1 → LUMO+2 HOMO → LUMO+1	0.59	π→π* π→π* π→π*	π→π*
353.12	3.5111	0.0182	HOMO-2 → LUMO HOMO-1 → LUMO+2 HOMO → LUMO+1	-0.22	π→π* π→π* π→π*	π→π*

Continued excitations of **HATN-2Me**

λ	E	*f*	Transition	Coefficients	Major Contributors	Assignment
336.85	3.6806	0.0571	HOMO-7 → LUMO HOMO-2 → LUMO+2 HOMO-1 → LUMO+2 HOMO → LUMO+1	0.11	π→π* π→π* π→π* π→π*	π→π*
335.69	3.6935	0.0777	HOMO-6 → LUMO HOMO-2 → LUMO+1 HOMO-1 → LUMO+1 HOMO → LUMO+2	0.25	π→π* π→π* π→π* π→π*	π→π*
328.04	3.7796	0.4069	HOMO-7 → LUMO HOMO-2→ LUMO+2 HOMO-1 → LUMO+2 HOMO → LUMO+1	0.63	π→π* π→π* π→π* π→π*	π→π*
327.90	3.7811	0.7275	HOMO-6 → LUMO HOMO-2 → LUMO+1 HOMO-1 → LUMO+1 HOMO → LUMO+2	-0.16	π→π* π→π* π→π* π→π*	π→π*

Continued excitations of **HATN-2Me**

λ	E	*f*	Transition	Coefficients	Major Contributors	Assignment
315.38	3.9313	0.7414	HOMO-6 → LUMO HOMO-2→ LUMO+1 HOMO-1 → LUMO+1 HOMO → LUMO+2	0.20	π→π* π→π* π→π* π→π*	π→π*

Table 13 First 10 excitations of HATN-4Br2Me

λ	E	*f*	Transition	Coefficients	Major Contributors	Assignment
413.82	2.9961	0.2219	HOMO →LUMO	0.68	π→π*	π→π*
410.35	3.0214	0.1001	HOMO-2 → LUMO+1 HOMO-1 → LUMO	-0.11	π→π* π→π*	π→π*
386.02	3.2119	0.0915	HOMO-2→ LUMO HOMO-1 → LUMO+1 HOMO → LUMO+2	0.68	π→π* π→π* π→π*	π→π*
384.41	3.2253	0.0051	HOMO-7 → LUMO HOMO-5 → LUMO+1 HOMO-3→ LUMO HOMO-3 → LUMO+2	0.62	n→π* n→π* n→π* n→π*	n→π*
376.60	3.2922	0.0244	HOMO-1 → LUMO+2 HOMO → LUMO+1	0.21	π→π* π→π*	π→π*
366.03	3.3873	0.1776	HOMO-2→ LUMO HOMO-1 → LUMO+1 HOMO→ LUMO+2	0.17	π→π* π→π* π→π*	π→π*

Continued excitations of **HATN-4Br2Me**

λ	E	*f*	Transition	Coefficients	Major Contributors	Assignment
351.47	3.5276	0.2447	HOMO-4 → LUMO HOMO-2→ LUMO+2 HOMO-1 → LUMO+1 HOMO → LUMO+2		π→π* π→π* π→π* π→π*	
347.89	3.5639	0.0846	HOMO-6 → LUMO HOMO-2 → LUMO+1 HOMO-1 → LUMO+2 HOMO → LUMO+1	0.59	π→π* π→π* π→π* π→π*	
344.46	3.5994	0.1599	HOMO-4 → LUMO HOMO-1 → LUMO+1 HOMO → LUMO+2	-0.24	π→π* π→π* π→π*	

Continued excitations of **HATN-4Br2Me**

λ	E	*f*	Transition	Coefficients	Major Contributors	Assignment
338.99	3.6574	0.6651	HOMO-6 → LUMO HOMO-2 → LUMO+1 HOMO-1 → LUMO+2 HOMO → LUMO+1	0.14	π→π* π→π* π→π* π→π*	

Table 14 First 10 excitations of HATN-2Br

λ	E	*f*	Transition	Coefficients	Major Contributors	Assignment
396.36	3.1281	0.2790	HOMO-2 →LUMO+2 HOMO → LUMO	0.12	π→π* π→π*	π→π*
395.66	3.1336	0.0363	HOMO-1 → LUMO	0.67	π→π*	π→π*
384.20	3.2271	0.0050	HOMO-6 → LUMO HOMO-6→ LUMO+1 HOMO-4→ LUMO HOMO-4 → LUMO+1 HOMO-3 → LUMO+2	0.68	n→π* n→π* n→π* n→π* n→π*	n→π*
378.62	3.2746	0.0168	HOMO-2 - HOMO-1 HOMO-1 → LUMO+1 HOMO → LUMO+2	0.58	π→π* π→π* π→π*	π→π*
353.86	3.5038	0.0065	HOMO-2 → LUMO HOMO-1 → LUMO+1 HOMO → LUMO+2	-0.12	π→π* π→π* π→π*	π→π*

Continued excitations of **HATN-2Br**

λ	E	*f*	Transition	Coefficients	Major Contributors	Assignment
341.65	3.6289	0.0377	HOMO-5 → LUMO HOMO-2 → LUMO+2 HOMO-1 > LUMO+2 HOMO → LUMO+1	0.21	π→π* π→π* π→π* π→π*	π→π*
338.67	3.6609	0.0318	HOMO-7 → LUMO HOMO-2 → LUMO+1 HOMO-1 → LUMO+1 HOMO → LUMO+2	0.19	π→π* π→π* π→π* π→π*	π→π*
333.33	3.7195	0.4086	HOMO-5 → LUMO HOMO-1 → LUMO+2 HOMO → LUMO+1	-0.18	π→π* π→π* π→π*	π→π*
328.62	3.7729	0.5194	HOMO-7→ LUMO HOMO-2 → LUMO+1 HOMO-1 → LUMO+1 HOMO → LUMO+2	0.64	π→π* π→π* π→π* π→π*	π→π*
320.69	3.8662	1.1461	HOMO-5 → LUMO HOMO-2 → LUMO+2 HOMO → LUMO+1	0.17	π→π* π→π* π→π*	π→π*

Table 15 First 10 excitations of HATN-4Me2Br

λ	E	*f*	Transition	Coefficients	Major Contributors	Assignment
412.00	3.0094	0.0400	HOMO →LUMO	0.68	π→π*	π→π*
403.61	3.0718	0.3113	HOMO-1 → LUMO	0.67	π→π*	π→π*
384.40	3.2254	0.0175	HOMO-2→ LUMO HOMO-1 → LUMO+2 HOMO → LUMO+1	0.62	π→π* π→π* π→π*	π→π*
3.2483	381.68	0.0050	HOMO-7 → LUMO HOMO-4→ LUMO HOMO-4→ LUMO+1 HOMO-3→ LUMO+2	-0.15	π→π* n→π* n→π* n→π*	n→π*
3.3496	370.15	0.0117	HOMO-1 → LUMO+1 HOMO → LUMO+2	0.24	π→π* π→π*	π→π*
360.74	3.4369	0.0687	HOMO-2 → LUMO HOMO-1 → LUMO+2 HOMO → LUMO+1	0.56	π→π* π→π* π→π*	π→π*

Continued excitations of **HATN-4Me2Br**

λ	E	*f*	Transition	Coefficients	Major Contributors	Assignment
347.54	3.5675	0.1241	HOMO-5 → LUMO HOMO-2 → LUMO+2 HOMO-1 → LUMO+1 HOMO → LUMO+2	0.27	π→π* π→π* π→π* π→π*	π→π*
342.65	3.6184	0.0953	HOMO-6 → LUMO HOMO-2 → LUMO+1 HOMO-1 → LUMO+2 HOMO → LUMO+1	0.19	π→π* π→π* π→π* π→π*	π→π*
339.91	3.6475	0.2500	HOMO-5 → LUMO HOMO-2 → LUMO+2 HOMO-1 → LUMO+1 HOMO → LUMO+2	-0.20	π→π* π→π* π→π* π→π*	π→π*
335.44	3.6961	0.6342	HOMO-6→ LUMO HOMO-2 → LUMO+1 HOMO-1 → LUMO+2 HOMO → LUMO+1	0.51	π→π* π→π* π→π* π→π*	π→π*

Table 16 First 10 excitations of HATN-4Me1COOH

λ	E	*f*	Transition	Coefficients	Major Contributors	Assignment
411.19	3.0152	0.0348	HOMO →LUMO	0.69	π→π*	π→π*
398.75	3.1093	0.2236	HOMO-1 → LUMO	0.67	π→π*	π→π*
384.26	3.2266	0.0047	HOMO-5→ LUMO	0.45	n→π*	n→π*
			HOMO-4 → LUMO		n→π*	
			HOMO-4 → LUMO+1		n→π*	
			HOMO-3 → LUMO+1		n→π*	
			HOMO-3→ LUMO+2		n→π*	
381.72	3.2480	0.0305	HOMO-2 → LUMO	-0.35	π→π*	π→π*
			HOMO-1→ LUMO+2		π→π*	
			HOMO → LUMO+1		π→π*	
			HOMO → LUMO+2		π→π*	
369.13	3.3588	0.0342	HOMO-1→ LUMO+1	-0.21	π→π*	π→π*
			HOMO-1→ LUMO+2		π→π*	
			HOMO → LUMO+1		π→π*	
			HOMO → LUMO+2		π→π*	

Continued excitations of **HATN-4Me1COOH**

λ	E	*f*	Transition	Coefficients	Major Contributors	Assignment
359.61	3.4477	0.0914	HOMO-2→ LUMO HOMO-1→ LUMO+1 HOMO-1→ LUMO+2 HOMO → LUMO+1 HOMO → LUMO+2	0.22	π→π* π→π* π→π* π→π* π→π*	π→π*
344.68	3.5971	0.0478	HOMO-6→ LUMO HOMO-2→ LUMO+1 HOMO-2→ LUMO+2 HOMO-1→ LUMO+1 HOMO-1→ LUMO+2 HOMO → LUMO+1 HOMO → LUMO+2	-0.18	π→π* π→π* π→π* π→π* π→π* π→π* π→π*	π→π*
339.59	3.6510	0.3668	HOMO-7 → LUMO HOMO-6→ LUMO HOMO-2→ LUMO+1 HOMO-2→ LUMO+2 HOMO-1→ LUMO+1 HOMO → LUMO+2	0.60	π→π* π→π* π→π* π→π* π→π* π→π*	π→π*

Continued excitations of **HATN-4Me1COOH**

λ	E	*f*	Transition	Coefficients	Major Contributors	Assignment
335.80	3.6922	0.2187	HOMO-7→1 LUMO HOMO-6→ LUMO HOMO-2→ LUMO+2 HOMO → LUMO+1 HOMO → LUMO+2	0.13	π→π* π→π* π→π* π→π* π→π*	π→π*
333.21	3.7208	0.6019	HOMO-7→ LUMO HOMO-6→ LUMO HOMO-2→ LUMO+1 HOMO-2→ LUMO+2 HOMO-1→ LUMO+1 HOMO-1→ LUMO+2 HOMO → LUMO+1 HOMO → LUMO+2	-0.24	π→π* π→π* π→π* π→π* π→π* π→π* π→π* π→π*	π→π*

Table 17 First 10 excitations of HATN-1COOH

λ	E	*f*	Transition	Coefficients	Major Contributors	Assignment
394.86	3.1399	0.0282	HOMO →LUMO	0.68094	π→π*	π→π*
389.92	3.1798	0.1841	HOMO-1 → LUMO	0.67111	π→π*	π→π*
387.28	3.2014	0.0050	HOMO-5→ LUMO	0.49504	n→π*	n→π*
			HOMO-4→ LUMO	0.30187	n→π*	
			HOMO-4→ LUMO+1	0.20695	n→π*	
			HOMO-3→ LUMO+1	0.20628	n→π*	
			HOMO-3→ LUMO+2	-0.17603	n→π*	
373.92	3.3158	0.0375	HOMO-2 → LUMO	0.62781	π→π*	π→π*
			HOMO-1→ LUMO+1	0.11167	π→π*	
			HOMO → LUMO+1	0.16589	π→π*	
			HOMO → LUMO+2	0.12751	π→π*	
361.55	3.4293	0.0180	HOMO-1→ LUMO+1	-0.37720	π→π*	π→π*
			HOMO-1 → LUMO+2	-0.33125	π→π*	
			HOMO → LUMO+1	0.39075	π→π*	
			HOMO → LUMO+2	-0.27997	π→π*	

Continued excitations of **HATN-1COOH**

λ	E	*f*	Transition	Coefficients	Major Contributors	Assignment
			HOMO-2→ LUMO	-0.23758	π→π*	
			HOMO-2→ LUMO+1	-0.10605	π→π*	
			HOMO-1→ LUMO+1	0.40829	π→π*	
351.79	3.5243	0.0273	HOMO-1→ LUMO+2	-0.27134	π→π*	π→π*
			HOMO → LUMO+1	0.32144	π→π*	
			HOMO → LUMO+2	0.24209	π→π*	
			HOMO-3 → LUMO	-0.15117	n→π*	
			HOMO-6→ LUMO	-0.28419	π→π*	
			HOMO-2→ LUMO+1	0.52152	π→π*	
			HOMO-2→ LUMO+2	-0.12424	π→π*	
338.98	3.6575	0.0045	HOMO-1→ LUMO+1	0.11081	π→π*	π→π*
			HOMO-1→ LUMO+2	0.11370	π→π*	
			HOMO → LUMO+1	0.15075	π→π*	
			HOMO → LUMO+2	-0.19527	π→π*	

Continued excitations of **HATN-1COOH**

λ	E	*f*	Transition	Coefficients	Major Contributors	Assignment
			HOMO-7→ LUMO	-0.29855	π→π*	
			HOMO-2→ LUMO+1	0.18501	π→π*	
			HOMO-2→ LUMO+2	0.34110	π→π*	
333.51	3.7175	0.2134	HOMO-1→ LUMO+1	-0.19758	π→π*	π→π*
			HOMO-1→ LUMO+2	0.12287	π→π*	
			HOMO → LUMO+1	0.12187	π→π*	
			HOMO → LUMO+2	0.36845	π→π*	
			HOMO-7→ LUMO	-0.16130	π→π*	
			HOMO-6→ LUMO	0.35754	π→π*	
			HOMO-2→ LUMO+2	0.24141	π→π*	
329.06	3.7678	0.2869	HOMO-1→ LUMO+1	0.25005	π→π*	π→π*
			HOMO-1→ LUMO+2	0.23870	π→π*	
			HOMO → LUMO+1	0.16957	π→π*	
			HOMO →LUMO+2	-0.32621	π→π*	

Continued excitations of **HATN-1COOH**

λ	E	*f*	Transition	Coefficients	Major Contributors	Assignment
			HOMO-7 →LUMO	-0.13650	π→π*	
			HOMO-6 → LUMO	-0.13698	π→π*	
			HOMO-2 → LUMO+1	-0.26362	π→π*	
325.29	3.8115	0.5410	HOMO-2 → LUMO+2	-0.31873	π→π*	π→π*
			HOMO-1 → LUMO+1	-0.12746	π→π*	
			HOMO-1 → LUMO+2	0.39004	π→π*	
			HOMO → LUMO+1	0.26631	π→π*	

Appendix C

C.1 Crystal Data

Table 18 Selected bond lengths for HATN-2Me-2ReS

Bond	Bond length (Å)	Bond	Bond length (Å)	Bond	Bond length (Å)
Re1-Br1A	2.6006(8)	Re2-N2	2.181(4)	O5- C31	1.139(7)
Re1-Br1B	2.36(2)	Re2-C31	1.935(5)	C27- O1	1.151(7)
Re1- C29	1.909(7)	Re2-N3	2.201(4)	N3-C23	1.331(7)
Re1-N6	2.191(4)	Re2-C30	1.914(6)	N3-C13	1.362(6)
Re1-C27	1.934(6)	C32-O6	1.150(8)	N1-C7	1.375(7)
Re1-N1	2.183(4)	C29-O3	1.150(8)	N1-C21	1.323(6)
Re1-C28	1.928(6)	N6-C26	1.337(7)	N4-C12	1.363(7)
Re2-Br2A	2.6043(8)	N6-C18	1.376(7)	N4-C24	1.326(7)
Re2-Br2B	2.42(2)	N2-C22	1.336(6)	N5-C19	1.349(7)
Re2-C32	1.918(7)	N2-C6	1.379(6)		

Table 19 Selected bond angles for HATN-2Me-2ReS

Bond	Bond angle (°)	Bond	Bond angle (°)
Br1B-Re1-Br1A	171.5(8)	C22-N2-Re2	111.7(3)
C29-Re1-Br1A	179.4(2)	C22-N2-C6	116.3(5)
C29-Re1-Br1B	8.5(9)	C27-Re1-Br1A	87.40(18)
C29-Re1-N6	97.1(3)	C27-Re1-Br1B	96.5(9)
C29-Re1-C27	92.1(3)	C27-Re1-N6	98.4(2)
C29-Re1-N1	96.3(3)	C6-N2-Re2	131.1(4)
C29-Re1-C28	89.6(3)	O1-C27-Re1	178.0(5)
N6-Re1-Br1A	82.66(12)	O5-C31-Re2	177.8(5)
N6-Re1-Br1B	89.3(8)	C23-N3-Re2	111.0(3)
C27-Re1-N1	169.9(2)	C23-N3-C13	117.7(5)
N1-Re1-Br1A	84.20(12)	C13-N3-Re2	129.7(4)
N1-Re1-Br1B	91.1(9)	N6-C26-C25	121.9(5)
N1-Re1-N6	74.92(17)	N6-C26-C21	116.6(5)
C28-Re1-Br1A	90.7(2)	C7-N1-Re1	130.8(4)
C28-Re1-Br1B	97.1(8)	C21-N1-Re1	111.9(3)
C28-Re1-N6	171.4(2)	C21-N1-C7	116.2(5)
C28-Re1-C27	86.7(3)	N5-C25-C26	121.8(5)
C28-Re1-N1	99.1(2)	N5-C25-C24	119.8(5)
C32-Re2-Br2A	178.5(2)	N1-C7-C8	120.1(5)
C32-Re2-Br2B	10.1(8)	N1-C7-C6	121.5(5)
C32-Re2-N2	96.2(2)	N3-C23-C24	121.5(5)
C32-Re2-C31	91.7(3)	N3-C23-C22	116.6(5)
C32-Re2-N3	99.2(2)	N4-C12-C11	119.4(5)
N2-Re2-Br2A	83.97(12)	N4-C12-C13	121.4(5)
N2-Re2-Br2B	89.1(7)	N4-C24-C25	120.0(5)
N2-Re2-N3	75.08(16)	N4-C24-C23	122.1(5)
C31-Re2-Br2A	88.34(17)	N1-C21-C26	117.9(5)
C31-Re2-Br2B	97.8(7)	N1-C21-C22	122.9(5)
C31-Re2-N2	170.0(2)	N2-C22-C23	118.0(5)
C31-Re2-N3	97.6(2)	N2-C22-C21	122.3(5)

Selected bond angles for HATN-2Me-2ReS Continued

Bond	Bond angle (°)	Bond	Bond angle (°)
N3-Re2-Br2A	82.26(12)	N3-C13-C12	119.7(5)
N3-Re2-Br2B	90.4(7)	N3-C13-C14	121.2(5)
C30-Re2-Br2A	89.05(19)	N2-C6-C7	120.5(5)
C30-Re2-Br2B	97.7(7)	N2-C6-C5	119.8(5)
C30-Re2-C32	89.5(3)	N6-C18-C19	119.5(5)
C30-Re2-N2	98.4(2)	N6-C18-C17	120.1(5)
C30-Re2-C31	87.8(2)	N5-C19-C18	123.4(5)
C30-Re2-N3	169.6(2)	N5-C19-C20	118.4(5)
O6-C32-Re2	175.8(7)	O4-C30-Re2	179.1(6)
O3-C29-Re1	177.3(7)	O2-C28-Re1	178.4(6)
C26-N6-Re1	111.3(3)	C18-N6-Re1	130.6(4)
		C26-N6-C18	116.7(5)

Table 20 Selected bond lengths for HATN-4Me-1ReS

Bond	Bond length (Å)	Bond	Bond length (Å)	Bond	Bond length (Å)
Re1 -C27	2.030(7)	N5 -C23	1.334(8)	O1- C25	1.160(9)
Re1 -Br1	2.5854(8)	N3 -C21	1.337(8)	N6 -C24	1.323(9)
Re1 -N3	2.192(5)	N3 -C16	1.367(8)	N6 -C17	1.356(8)
Re1 -N2	2.194(5)	O2 -C26	1.154(8)	N1 -C14	1.360(8)
Re1 -C25	1.916(8)	N4 -C15	1.348(8)	N1 -C19	1.310(8)
Re1 -C26	1.919(7)	N4 -C22	1.325(8)	N2 -C20	1.342(8)
C27 -O3	0.988(7)	N5 -C18	1.359(9)	N2 -C13	1.353(8)

Table 21 Selected bond angles for HATN-4Me-1ReS

Bond	Bond angle (°)	Bond	Bond angle (°)
C27-Re1-Br1	176.12(17)	O1-C25-Re1	176.6(7)
C27-Re1-N3	93.0(2)	N5-C18-C17	121.5(6)
C27-Re1-N2	93.3(2)	N5-C18-C9	119.3(6)
N3-Re1-Br1	83.74(14)	C17-C18-C9	119.2(6)
N3-Re1-N2	74.9(2)	N6-C24-C23	122.2(6)
N2-Re1-Br1	83.78(14)	N6-C24-C19	117.3(6)
C25-Re1-C27	93.1(3)	C23-C24-C19	120.4(6)
C25-Re1-Br1	90.0(2)	N2-C20-C21	117.1(6)
C25-Re1-N3	172.0(2)	N2-C20-C19	121.8(6)
C25-Re1-N2	99.5(3)	N1-C14-C13	121.0(6)
C25-Re1-C26	86.3(3)	N6-C17-C18	121.4(6)
C26-Re1-C27	92.8(3)	N6-C17-C12	119.0(6)
C26-Re1-Br1	89.8(2)	N1-C19-C24	119.9(6)
C26-Re1-N3	98.6(3)	N1-C19-C20	121.9(6)
C26-Re1-N2	171.3(2)	N3-C16-C15	119.2(6)
O3-C27-Re1	178.9(6)	N3-C16-C5	122.1(6)
C23-N5-C18	116.6(6)	N4-C15-C16	122.2(6)
C21-N3-Re1	113.8(4)	N4-C15-C8	119.6(6)
C21-N3-C16	117.2(5)	N4-C22-C21	121.4(6)
C16-N3-Re1	128.5(4)	N4-C22-C23	119.3(6)
C22-N4-C15	117.4(5)	C21-C22-C23	119.3(6)
C20-N2-Re1	113.6(4)	N2-C13-C14	120.2(6)
C20-N2-C13	117.1(6)	N2-C13-C4	122.5(6)
C13-N2-Re1	129.1(4)	O2-C26-Re1	177.5(6)
C24-N6-C17	116.8(6)	N5-C23-C24	121.6(6)
N3-C21-C20	116.7(6)	N5-C23-C22	118.4(6)
N3-C21-C22	122.3(6)	N1-C14-C1	119.4(6)
C19-N1-C14	117.5(6)		

Table 22 Selected bond lengths for HATN-4Me-1ReA

Bond	Bond length (Å)	Bond	Bond length (Å)	Bond	Bond length (Å)
Re1-N2	2.206(17)	N3-C25	1.40(2)	N6-C16	1.38(2)
Re1-N3	2.206(19)	N3-C11	1.38(2)	C28-N6	1.37(2)
Re1-C29	2.01(3)	N1-C23	1.37(2)	O6-C61	1.19(3)
Re1-Br1	2.612(3)	N1-C5	1.36(3)	N7-C36	1.44(2)
Re1-C30	1.88(2)	N9-C42	1.45(2)	N7-C53	1.38(2)
Re1-C31	1.95(3)	N9-C55	1.34(2)	C35-N8	1.39(2)
Re2-Br2	2.618(3)	O4-C59	1.11(2)	C10-C9	1.3900
Re2-N9	2.158(19)	N12-C58	1.40(2)	C10-C11	1.3900
Re2-C59	1.84(2)	N12-C46	1.41(2)	C10-N4	1.41(2)
Re2-C61	1.90(2)	N10-C41	1.36(2)	C17-N5	1.39(4)
Re2-N8	2.183(19)	N10-C56	1.40(2)	C54-N8	1.41(2)
Re2-C60	1.86(2)	N11-C57	1.38(2)	O5-C60	1.14(3)
N2-C24	1.44(2)	N11-C47	1.35(2)	O2-C30	1.21(3)
N2-C4	1.30(3)	C27-N5	1.36(2)	O3-C31	1.14(3)
O1-C29	1.03(3)	C26-N4	1.34(2)		

Table 23 Selected bond angles for HATN-4Me-1ReA

Bond	Bond angle (°)	Bond	Bond angle (°)
N2-Re1-N3	75.6(10)	C58-N12-C46	116(3)
N2-Re1-Br1	82.6(7)	C41-N10-C56	119(3)
N3-Re1-Br1	84.5(8)	C57-N11-C47	117(2)
C29-Re1-N2	97.4(13)	N5-C27-C26	122(2)
C29-Re1-N3	96.8(13)	N5-C27-C28	118(2)
C29-Re1-Br1	178.6(11)	N4-C26-C27	120(2)
C30-Re1-N2	171.5(15)	N4-C26-C25	119(2)
C30-Re1-N3	98.4(15)	C26-C25-N3	121.3(19)
C30-Re1-C29	89.3(17)	C24-C25-N3	118.7(19)
C30-Re1-Br1	90.9(13)	C25-C24-N2	116.2(18)
C31-Re1-N2	98.6(13)	C23-C24-N2	123.6(18)
C31-Re1-N3	172.3(13)	N1-C23-C24	117.4(19)
C31-Re1-C29	88.8(16)	N1-C23-C28	122.4(19)
C31-Re1-Br1	89.8(12)	N6-C28-C27	121(2)
C31-Re1-C30	86.8(17)	N6-C28-C23	119(2)
N9-Re2-Br2	82.3(9)	N8-C35-C34	119.2(17)
N9-Re2-N8	75.7(11)	N8-C35-C36	120.8(17)
C59-Re2-Br2	175.4(9)	N7-C36-C35	122.1(18)
C59-Re2-N9	101.1(13)	N7-C36-C37	117.7(18)
C59-Re2-C61	91.9(13)	C16-N6-C28	125(2)
C59-Re2-N8	94.8(11)	O1-C29-Re1	115(2)
C61-Re2-Br2	90.6(10)	C9-C10-C11	117.0(18)
C61-Re2-N9	98.8(13)	N4-C10-C9	122.7(18)
C61-Re2-N8	172.1(12)	N4-C10-C11	119.0(17)
N8-Re2-Br2	83.0(7)	N3-C11-C10	121.0(17)
C60-Re2-Br2	86.7(14)	N3-C11-C12	118(2)
C60-Re2-N9	166.7(16)	N5-C17-C18	122(2)
C60-Re2-C59	89.5(16)	N5-C17-C16	121(2)
C60-Re2-C61	88.6(16)	N6-C16-C17	119(2)
C60-Re2-N8	95.7(15)	N7-C53-C54	122(3)
C24-N2-Re1	112.7(18)	C53-C54-N8	120(3)

Selected bond angles for HATN-4Me-1ReA continued

Bond	Bond angle (°)	Bond	Bond angle (°)
C24-N2-Re1	112.7(18)	C53-C54-N8	120(3)
C4-N2-Re1	130.7(19)	C55-C54-N8	172(4)
C4-N2-C24	116(2)	N9-C55-C56	120.0
C25-N3-Re1	110.1(18)	N9-C55-C54	117(2)
C11-N3-Re1	130(2)	N1-C5-C6	123(2)
C11-N3-C25	119(2)	N1-C5-C4	117.9(19)
C5-N1-C23	120(2)	C5-C4-N2	122.0(19)
C42-N9-Re2	131(2)	C3-C4-N2	121(2)
C55-N9-Re2	116(2)	N11-C47-C48	119(2)
C55-N9-C42	113(3)	N11-C47-C46	119(2)
N6-C16-C15	121(2)	N12-C46-C47	119.8(18)
O4-C59-Re2	179(3)	N12-C46-C45	121.8(17)
N10-C41-C40	118(2)	C27-N5-C17	118.1(17)
N10-C41-C42	122(2)	O6-C61-Re2	177(3)
C71-C42-N9	119.4(19)	C26-N4-C10	118(3)
C41-C42-N9	120.5(19)	C35-N8-Re2	133.0(18)
N10-C56-C57	120.3(18)	C35-N8-C54	116(2)
N10-C56-C55	119.0(18)	C54-N8-Re2	111.2(17)
N11-C57-C56	119.1(18)	O2-C30-Re1	174(4)
N11-C57-C58	120.7(18)	O3-C31-Re1	175(4)
N12-C58-C57	122.6(19)	O5-C60-Re2	169(4)
N12-C58-C53	117.4(19)	N7-C53-C58	120.1(18)

Appendix D

D.1 UV/Visible spectroscopy

Solution UV-Visible absorbance spectra were recorded on a Shimadzu UV-3101PC UV-VIS-NIR-scanning spectrophotometer. Samples were recorded in chloroform at concentrations near 10^{-6} M.

D.2 Vibrational spectroscopy

All ground state vibrational measurements were taken in the solid state on a Nicolet 5700 FT-IR from Thermo Electron Corporation using an ATR attachment. Continuous wave excitation was used for all Raman measurements. Raman spectroscopy was carried out on the Bruker Equinox 55 interferometer equipped with the Bruker FRA 106/S FT-Raman accessory, with the source Nd:YAG laser at 1064 nm. The defocused aperture setting that gave a 1 mm diameter spot size was used, with a power setting of 120 mW and a resolution of 4 cm^{-1}. 120 scans were co-added to produce a spectrum with an acceptable signal/noise ratio.

D.3 EPR Measurements

EPR spectra were recorded at 110 K on a Varian E-104A spectrometer equipped with a E-257 variable-temperature controller and operating at about 9.0 GHz. The spectral *g* values were calibrated with (diphenylpicryl)hydrazyl (DPPH) as a standard. Samples were recorded in DCM or acetonitrile at a concentration of 5 mM.

D.4 Electrochemistry methods

Solution state (staircase) cyclic voltammetry (CV) measurements were performed using a three electrode system comprised of a macro platinum working electrode, a macro platinum auxiliary (counter) electrode and a silver/silver chloride (Ag/AgCl) reference

electrode. CV measurements were performed on 0.5 x10^{-4} mM solutions using 0.1 M tetra-*n*-butylammonium bromide (TBABr) as the supporting electrolyte. A reference CV of ferrocene in 0.1 M TBABr was acquired. Using literature values for the ferrocene redox couple with respect to a Ag/AgCl reference electrode all potential values are reported with respect to a Fc/Fc+ reference electrode.[2,3]

Literature values reported with respect to reference electrodes other than a Fc/Fc+ electrode (i.e the normal hydrogen electrode (NHE)) have been converted to be with respect to a Fc/Fc+ electrode to make comparisons with the potential values in this thesis. This conversion was achieved using literature values for the NHE electrodes.

To calculate electronic bandgaps for each molecule the HOMO potential was calculated from the cyclic voltammograms (with respect to Fc/Fc+). To convert the Eonsetox values into a HOMO potential, the following relationship was used:[4]

Ionisation Potential (HOMO) = Eonsetox (vs Fc/Fc+) + 4.4 eV

The bandgap was estimated from onset wavelength (λonset) of the lowest energy band in the absorption spectra. To calculate the bandgap, the UV-Vis onset wavelength was converted to energy (in eV) using Planck's equation E = hυ (where 1243 is the conversion factor to energy in eV):

$$\text{Band gap (eV)} = \frac{1243}{\lambda_{onset}(nm)}$$

This allowed a retrospective calculation of the LUMO potential of each compound.

D.5 Accuracy of calculation models (MAD values) for HATN-1Re complexes

Mean average deviation (MAD) is calculated between the experimental and calculated results for the complexes.

Table 24 MAD values between crystal structures bond lengths and DFT optimised structures bond lengths.

Compound	MAD Value
HATN-4Me-1ReA	0.077
HATN-4Me-1ReS	0.029

Table 25 Rhenium complex MAD values for IR and FT-Raman experimental and calculated data.

Complex	MAD value FT-IR	MAD value FT-R
HATN-4Me-1ReS	9	18
HATN-2Me-1ReA	11	16
HATN-2Br-1ReS	14	13
HATN-2Br-1ReA	12	14
HATN-4Br2Me-1ReA	13	
HATN-4Me2Br-1ReS	12	13
HATN-4Br-1ReS	10	12
HATN-4Me-2ReA	12	15
HATN-2Me-2ReS	11	18
HATN-4Br2Me-2ReS	12	12
HATN-4Me2Br-2ReA	13	

D.6 FT-Raman spectra of HATN-Re complexes

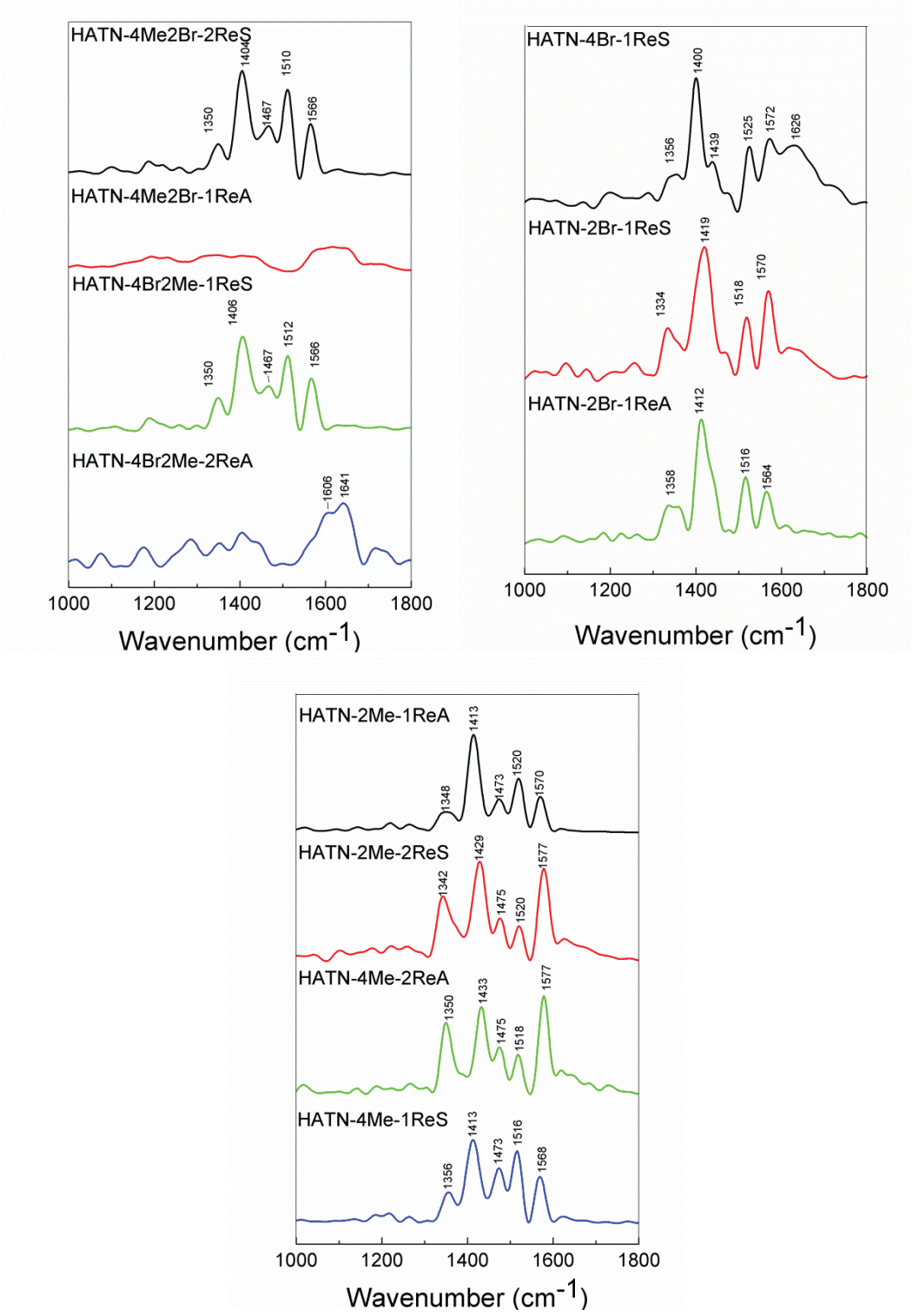

Figure 1 FT-Raman spectra of HATN-Re complexes.

D.7 HATN-Re FT-IR spectra

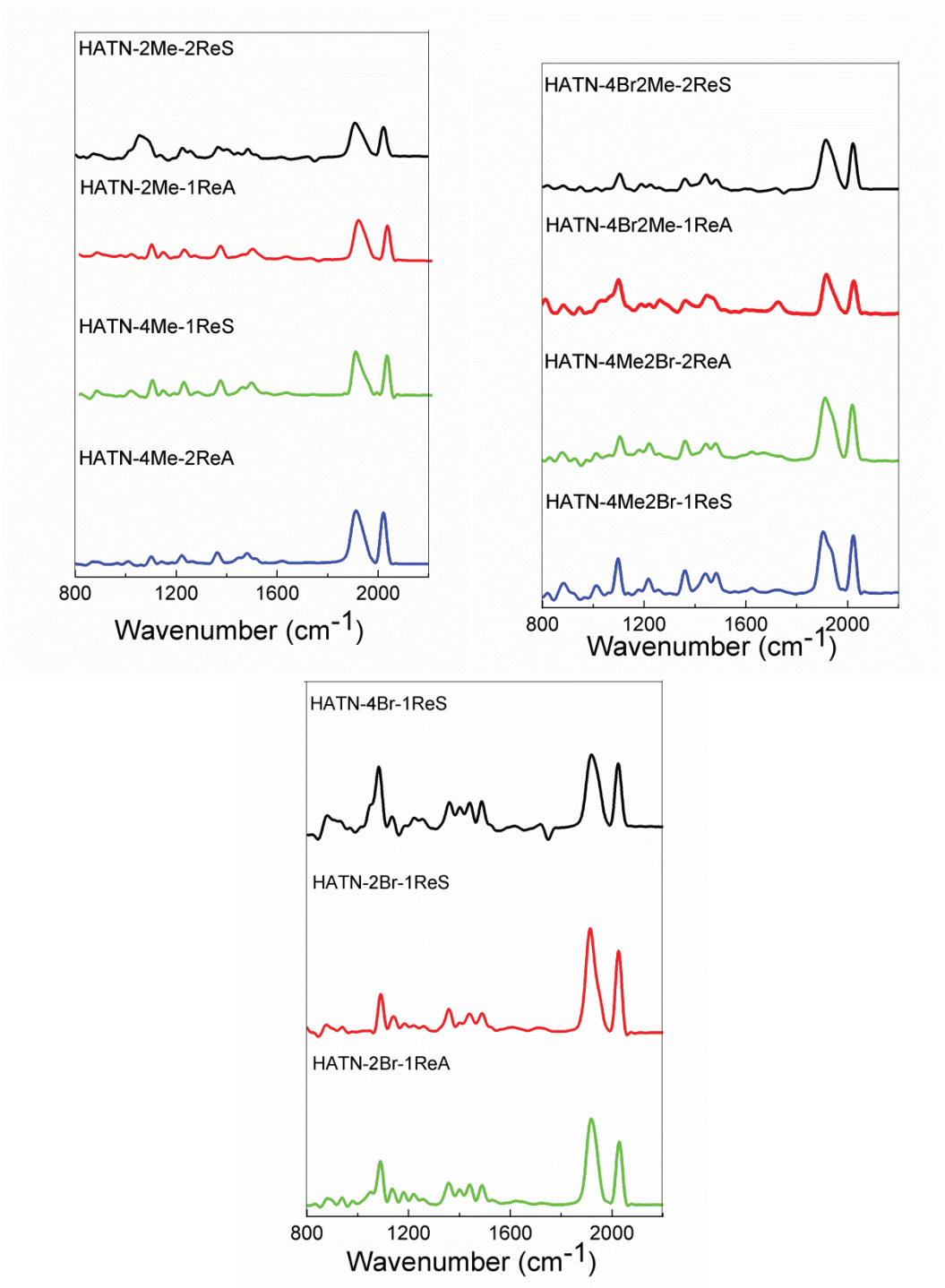

Figure 2 FT-IR spectra of HATN-Re complexes

D.8 Excitation tables for HATN-1Re complexes

Table 26 Summary of the first ten transitions calculated for the complex HATN-4Me-1ReS. Only transitions with nonzero oscillator strengths are shown.

λ (nm)	E (eV)	*F*	Transition	Coefficients	Major Contributors	Assignment
666.44	1.8604	0.0200	HOMO-1 →LUMO	0.69843	Re→π*	MLCT
535.45	2.3155	0.0014	HOMO → LUMO+1	0.69783	Re→π*	MLCT
510.77	2.4274	0.0133	HOMO-1 → LUMO+1	0.70205	Re →π*	MLCT
503.99	2.4600	0.0021	HOMO-3 → LUMO HOMO -2→ LUMO	0.32319 0.61476	π→π* π→π*	π→π*
484.41	2.5595	0.0109	HOMO-1 → LUMO+2	0.70045	Re →π*	MLCT
460.04	2.6951	0.0089	HOMO-8 → LUMO HOMO-5→ LUMO HOMO-4→ LUMO	0.18132 0.23929 0.63353	Re →π* π→π* Re→π*	MLCT
451.05	2.7488	0.0206	HOMO-4 → LUMO+1 HOMO-3→ LUMO HOMO -2→ LUMO	-0.10520 0.60173 -0.30944	Re →π* π→π* π→π*	π→π*
417.75	2.9679	0.0840	HOMO-5 → LUMO HOMO-4→ LUMO HOMO-3→ LUMO+1	0.64174 -0.23120 -0.10501	π→π* Re→π* π→π*	π→π*
399.66	3.1023	0.0425	HOMO-6→ LUMO HOMO-3→ LUMO	0.67831 -0.10730	N→π* π→π*	N→π*
393.96	3.1471	0.0028	HOMO-8→ LUMO HOMO-4 → LUMO HOMO -2→ LUMO+1	0.52422 -0.10185 0.41847	Re →π* Re →π* π→π*	MLCT

Table 27 Summary of the first ten transitions calculated for the complex HATN-4Br-1ReS. Only transitions with nonzero oscillator strengths are shown.

λ (nm)	E (eV)	*F*	Transition	Coefficients	Major Contributors	Assignment
734.41	1.6882	0.0015	HOMO →LUMO	0.70439	Re →π*	MLCT
634.22	1.9549	0.0358	HOMO-1 → LUMO	0.69573	Re →π*	MLCT
521.96	2.3753	0.0031	HOMO-4 → LUMO	0.43128	π→π*	MLCT
			HOMO-3→ LUMO	0.52610	Re →π*	
			HOMO →LUMO+1	-0.16538	Re →π*	
501.42	2.4727	0.0064	HOMO-4→ LUMO	0.17742	π→π*	MLCT
			HOMO→ LUMO+1	0.67476	Re →π*	
470.03	2.6378	0.2406	HOMO-2 → LUMO	0.62223	π→π*	π→π*
			HOMO-1→ LUMO+1	0.31076	Re →π*	
468.86	2.6444	0.0019	HOMO-4 → LUMO	0.51541	π→π*	MLCT
			HOMO-3→ LUMO	-0.44786	Re →π*	
			HOMO→ LUMO+1	-0.10268	Re →π*	
458.30	2.7053	0.0251	HOMO-9→ LUMO	0.13255	Re →π*	π→π*
			HOMO-8→ LUMO	0.22036	π→π*	
			HOMO-5→ LUMO	0.64754	π→π*	
443.65	2.7946	0.0016	HOMO → LUMO+2	0.70252	Re →π*	MLCT
429.31	2.8880	0.0158	HOMO-1 → LUMO+2	0.69501	Re →π*	MLCT
416.42	2.9774	0.0653	HOMO-10 → LUMO	0.12992	π→π*	MLCT
			HOMO-7→ LUMO	0.66465	Re →π*	
			HOMO-4→ LUMO	-0.10286	π→π*	
			HOMO-2→ LUMO+1	0.11094	π→π*	

Table 28 Summary of the first ten transitions calculated for the complex HATN-2Me-1ReA. Only transitions with nonzero oscillator strengths are shown.

λ (nm)	E (eV)	*f*	Transition	Coefficients	Major Contributors	Assignment
649.26	1.9096	0.0014	HOMO →LUMO	0.70296	Re→π*	MLCT
578.56	2.1430	0.0391	HOMO-1 → LUMO	0.69626	Re→π*	MLCT
481.14	2.5769	0.0033	HOMO-5 → LUMO	0.13582	Re→π*	MLCT
			HOMO-4 → LUMO	0.51418	Re→π*	
			HOMO-3 → LUMO	-0.25198	Re→π*	
			HOMO-2 → LUMO	0.34432	Re→π*	
			HOMO → LUMO+1	0.15776	Re→π*	
464.22	2.6708	0.0069	HOMO-4 → LUMO	-0.19660	Re→π*	MLCT
			HOMO → LUMO+1	0.66978	Re→π*	
449.33	2.7593	0.0025	HOMO-5 → LUMO	-0.11974	Re→π*	MLCT
			HOMO-3 → LUMO	0.23151	Re→π*	
			HOMO-1 → LUMO+1	0.64528	Re→π*	
447.06	2.7733	0.0031	HOMO-4 → LUMO	-0.39434	Re→π*	MLCT
			HOMO-3 → LUMO	-0.14570	Re→π*	
			HOMO-2 → LUMO	0.53131	Re→π*	
			HOMO → LUMO+1	-0.13167	Re→π*	
436.32	2.8416	0.0106	HOMO-3 → LUMO	0.16785	Re→π*	MLCT
			HOMO → LUMO+2	0.67197	Re→π*	

Continued transitions for **HATN-2Me-1ReA**

λ (nm)	E (eV)	*f*	Transition	Coefficients	Major Contributors	Assignment
432.25	2.8683	0.1550	HOMO-8 → LUMO	0.15051	Re→π*	MLCT
			HOMO-5 → LUMO	-0.29580	Re→π*	
			HOMO-4 → LUMO	0.12139	Re→π*	
			HOMO-3 → LUMO	0.43634	Re→π*	
			HOMO-2 → LUMO	0.26043	Re→π*	
			HOMO-1 → LUMO+1	-0.24684	Re→π*	
			HOMO → LUMO+2	-0.19470	Re→π*	
427.05	2.9033	0.0107	HOMO-5→ LUMO	0.58019	Re→π*	MLCT
			HOMO-3 → LUMO	0.35229	Re→π*	
422.68	2.9333	0.0283	HOMO-1 →156	0.69995	Re→π*	MLCT

Table 29 Summary of the first ten transitions calculated for the complex HATN-2Br-1ReS. Only transitions with nonzero oscillator strengths are shown.

λ (nm)	E (eV)	*f*	Transition	Coefficients	Major Contributors	Assignment
678.01	1.8286	0.0015	HOMO →LUMO	0.69982	Re→π*	MLCT
595.66	2.0815	0.0417	HOMO-1 → LUMO	0.69408	Re→π*	MLCT
496.02	2.4996	0.0020	HOMO-3→ LUMO	0.36888	Re→π*	MLCT
			HOMO-2→ LUMO	0.54517	Re→π*	
			HOMO → LUMO+2	-0.23070	Re→π*	
482.75	2.5683	0.0086	HOMO-3 → LUMO	0.19305	Re→π*	MLCT
			HOMO-2→ LUMO	0.13581	Re→π*	
			HOMO → LUMO+2	0.65778	Re→π*	
464.05	2.6718	0.0184	HOMO-1 → LUMO+2	0.69203	Re→π*	MLCT
454.68	2.7269	0.0376	HOMO-1 → LUMO+1	0.69534	Re→π*	MLCT
444.57	2.7889	0.0033	HOMO-6→ LUMO	0.13188	Re→π*	MLCT
			HOMO-3→ LUMO	0.53946	Re→π*	
			HOMO-2→ LUMO	-0.39910	Re→π*	
437.52	2.8338	0.0273	HOMO-8 → LUMO	0.18482	Re→π*	MLCT
			HOMO-5→ LUMO	0.65002	Re→π*	
			HOMO-4→ LUMO	-0.15723	π→π*	
426.09	2.9098	0.0691	HOMO-5 → LUMO	0.17804	Re→π*	MLCT
			HOMO-4→ LUMO	0.67101	π→π*	
403.22	3.0749	0.1441	HOMO-9 → LUMO	-0.14693	π→π*	MLCT
			HOMO-6→ LUMO	0.64520	Re→π*	
			HOMO-4→ LUMO+2	-0.10136	π→π*	
			HOMO-3→ LUMO	-0.13737	Re→π*	

Table 30 Summary of the first ten transitions calculated for the complex HATN-2Br-1ReA. Only transitions with nonzero oscillator strengths are shown.

λ (nm)	E (eV) (eV)	*F*	Transition	Coefficients	Major Contributors	Assignment
825.99	1.5010	0.0011	HOMO→LUMO	0.70325	Re→π*	MLCT
681.21	1.8201	0.0247	HOMO-2 → LUMO	0.10626	π→π*	MLCT
			HOMO -1→ LUMO	0.69178	Re→π*	
538.56	2.3021	0.0044	HOMO-3 → LUMO	0.34695	Re→π*	MLCT
			HOMO -2→ LUMO	0.55105	π→π*	
			HOMO → LUMO+1	0.24697	Re→π*	
519.62	2.3861	0.0177	HOMO-1 → LUMO+1	0.69733	Re→π*	MLCT
492.59	2.5170	0.0067	HOMO-8→ LUMO	-0.14884	Re→π*	MLCT
			HOMO-5→ LUMO	-0.18017	Re→π*	
			HOMO-4→ LUMO	0.62119	Re→π*	
			HOMO-3→ LUMO	0.12669	Re→π*	
			HOMO → LUMO+2	-0.17903	Re→π*	
476.51	2.6019	0.0045	HOMO-4 → LUMO	-0.11208	Re→π*	MLCT
			HOMO-3 → LUMO	0.43491	Re→π*	
			HOMO-2→ LUMO	-0.23138	π→π*	
			HOMO-1→ LUMO+2	0.45849	Re→π*	
470.95	2.6327	0.0406	HOMO-4→ LUMO+1	0.10360	Re→π*	MLCT
			HOMO-3→ LUMO	-0.37185	Re→π*	
			HOMO-2→ LUMO	0.21355	π→π*	
			HOMO-1→ LUMO+2	0.53290	Re→π*	

Continued transitions for **HATN-2Br-1ReA**

λ (nm)	E (eV)	*f*	Transition	Coefficients	Major Contributors	Assignment
437.20	2.8359	0.0714	HOMO-5→ LUMO	0.66428	Re→π*	MLCT
			HOMO-4→ LUMO	0.17374	Re→π*	
422.28	2.9361	0.0010	HOMO-7→ LUMO	0.63758	Re→π*	MLCT
			HOMO-7→ LUMO+2	0.22458	Re→π*	
			HOMO-6→ LUMO	0.17566	n→π*	
414.65	2.9901	0.0401	HOMO-7 → LUMO	-0.17762	Re→π*	n→π*
			HOMO-6→ LUMO	0.66152	n→π*	

Table 31 Summary of the first ten transitions calculated for the complex HATN-4Br2Me-1ReA. Only transitions with nonzero oscillator strengths are shown.

λ (nm)	E (eV)	*f*	Transition	Coefficients	Major Contributors	Assignment
695.80	1.7819	0.0015	HOMO →LUMO	0.70060	Re→π*	MLCT
612.04	2.0257	0.0351	HOMO-1 → LUMO	0.69490	Re→π*	MLCT
504.23	2.4589	0.0017	HOMO-5 → LUMO	-0.10537	π→π*	MLCT
			HOMO-4 → LUMO	0.54193	Re→π*	
			HOMO-2 → LUMO	0.36651	Re→π*	
			HOMO → LUMO+1	-0.15107	Re→π*	
			HOMO → LUMO+2	0.14371	Re→π*	
490.43	2.5281	0.0063	HOMO-4 → LUMO	0.20457	Re→π*	MLCT
			HOMO → LUMO+1	0.53920	Re→π*	
			HOMO → LUMO+2	-0.38302	Re→π*	
472.92	2.6217	0.0050	HOMO-3 → LUMO	-0.16335	π→π*	MLCT
			HOMO-2 → LUMO	-0.11077	Re→π*	
			HOMO-1 → LUMO+1	0.46078	Re→π*	
			HOMO-1 → LUMO+2	-0.34209	Re→π*	
			HOMO → LUMO+1	-0.24365	Re→π*	
			HOMO → LUMO+2	-0.24290	Re→π*	
471.64	2.6288	0.0030	HOMO-3 → LUMO	-0.11144	π→π*	MLCT
			HOMO-1 → LUMO+1	0.27325	Re→π*	
			HOMO-1 → LUMO+2	-0.19050	Re→π*	
			HOMO → LUMO+1	0.34045	Re→π*	
			HOMO → LUMO+2	0.49226	Re→π*	

Continued transitions for **HATN-4Br2Me-1ReA**

λ (nm)	E (eV)	*f*	Transition	Coefficients	Major Contributors	Assignment
467.23	2.6536	0.0167	HOMO-4 → LUMO	-0.33672	Re→π*	MLCT
			HOMO-3 → LUMO	0.14546	π→π*	
			HOMO-2 → LUMO	0.54062	Re→π*	
			HOMO-1 → LUMO+1	0.15110	Re→π*	
			HOMO → LUMO+2	-0.14569	Re→π*	
455.32	2.7230	0.0357	HOMO-2 → LUMO	-0.10206	Re→π*	MLCT
			HOMO-1 → LUMO+1	0.41217	Re→π*	
			HOMO-1 →LUMO+2	0.55305	Re→π*	
450.20	2.7540	0.1858	HOMO-7 → LUMO	-0.13495	Re→π*	π→π*
			HOMO-5→ LUMO	-0.33464	π→π*	
			HOMO-3 → LUMO	0.52068	π→π*	
			HOMO-2→ LUMO	-0.15583	Re→π*	
			HOMO-1 → LUMO+2	-0.17632	Re→π*	
438.74	2.8259	0.0803	HOMO-7 → LUMO	0.12079	Re→π*	π→π*
			HOMO-5 → LUMO	0.55374	π→π*	
			HOMO-4 → LUMO	0.13204	Re→π*	
			HOMO-3 → LUMO	0.36751	π→π*	

Table 32 Summary of the first ten transitions calculated for the complex HATN-4Me2Br-1ReS. Only transitions with nonzero oscillator strengths are shown.

λ (nm)	E (eV)	*F*	Transition	Coefficients	Major Contributors	Assignment
639.62	1.9384	0.0016	HOMO →LUMO	0.69693	Re→π*	MLCT
			HOMO → LUMO+1	-0.11223	Re→π*	
573.71	2.1611	0.0324	HOMO -1→ LUMO	0.69278	Re→π*	MLCT
468.70	2.6453	0.0059	HOMO -4 → LUMO	-0.32443	Re→π*	MLCT
			HOMO → LUMO+2	0.61273	Re→π*	
454.52	2.7278	0.0071	HOMO -3→ LUMO	-0.19685	π→π*	MLCT
			HOMO -1→ LUMO+2	0.67127	Re→π*	
454.24	2.7295	0.0539	HOMO -1 → LUMO+1	0.68488	Re→π*	MLCT
444.84	2.7872	0.0024	HOMO -4→ LUMO	-0.31473	Re→π*	π→π*
			HOMO -2→ LUMO	0.58978	π→π*	
			HOMO -1→ LUMO+1	0.13333	Re→π*	
			HOMO → LUMO+2	-0.10559	Re→π*	
435.90	2.8444	0.0994	HOMO -7 → LUMO	-0.13883	Re→π*	π→π*
			HOMO -5→ LUMO	-0.44816	π→π*	
			HOMO -3→ LUMO	0.47484	π→π*	
			HOMO -2→ LUMO+2	0.10492	π→π*	
			HOMO -1→ LUMO+2	0.18510	Re→π*	
422.42	2.9351	0.1355	HOMO -5 → LUMO	0.51343	π→π*	π→π*
			HOMO -3→ LUMO	0.45339	π→π*	

Continued transitions for **HATN-4Me2Br-1ReS**

λ (nm)	E (eV)	*f*	Transition	Coefficients	Major Contributors	Assignment
393.88	3.1478	0.0029	HOMO -8 → LUMO	0.53857	n→π*	n→π*
			HOMO -8→ LUMO+1	0.41732	n→π*	
			HOMO -6→ LUMO	0.11862	Re→π*	
391.90	3.1637	0.1683	HOMO -10 → LUMO	0.15361	Re→π*	MLCT
			HOMO -6→ LUMO	0.52264	Re→π*	
			HOMO -3→ LUMO+2	-0.25650	π→π*	
			HOMO -2→ LUMO+1	-0.31378	π→π*	

D.9 Experimental and calculated vibrational frequencies for HATN-1Re

Table 33 Experimental and calculated vibrational frequencies of HATN-4Me-1ReS for FT-IR and FT-Raman.

ν_{FT-R} /cm^{-1}	ν_{FT-IR} /cm^{-1}	ν_{Calc} /cm^{-1}	S/A	Assignment from GaussView
	1092	1077	S	In plane delocalised ring distortions with H-wag
	1217	1211	A	In plane delocalised ring distortions with H-wag
	1362	1347	A	In plane delocalised ring distortions, stronger on rings 1 and 2 with H-wag
	1448	1451	A	H-wag and Me(H) wag, weak ring distortions
	1485	1481	S	In plane delocalised ring distortions with H-wag
	1896	1932		Out of sync CO stretching
	2021	2018		In sync CO stretching
503		490		CO stretching
1356		1349	S	Strong in plane delocalised ring distortions with weak H-wag
1413		1406	A	In plane delocalised ring distortions, strong on rings 1 and 2 with H-wag
1473		1493	S	In plane delocalised ring distortions, strong in pyrazines 1 and 2 with H-wag
1516		1503	A	In plane delocalised ring distortions, strong in all pyrazines with H-wag
1568		1615	S	In plane delocalised ring distortions, stronger in rings 1 and 2 with H-wag

S/A indicates symmetric or asymmetric stretching

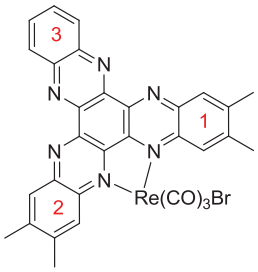

Table 34 Experimental and calculated vibrational frequencies of HATN-4Br-1ReS for FT-IR and FT-Raman.

$\nu_{FT\text{-}R}$ /cm^{-1}	$\nu_{FT\text{-}IR}$ /cm^{-1}	ν_{Calc} /cm^{-1}	S/A	Assignment from GaussView
	764	755	S	H-wag out of plane on ring 3
	1082	1077	A	In plane delocalised ring distortions with H-wag
	1360	1342	A	In plane delocalised ring distortions with H-wag
	1402	1421	S	In plane delocalised ring distortions, stronger on rings 1 and 2, with H-wag
	1440	1431	S	In plane delocalised ring distortions with H-wag
	1487	1487	S	In plane localised ring distortions on phenazines 1 and 2
	1919	1942		Out of sync CO stretching
	2023	2026		In sync CO stretching
1356		1370	S	In plane delocalised ring distortions, stronger on rings 1 and 2
1400		1380	S	In plane localised ring distortions on phenazines 3
1439		1421	S	In plane delocalised ring distortions, stronger on rings 1 and 2
1525		1525	A	In plane delocalised ring distortions, stronger on rings 1 and 2 with H-wag
1572		1568	A	In plane strong localised ring distortions on phenazines 3 with H-wag
1626		755	A	In sync CO stretching
2131		1077		In sync CO stretching

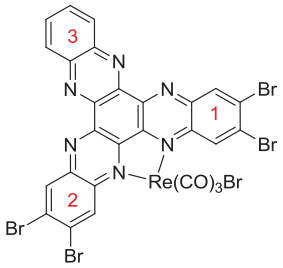

S/A indicates symmetric or asymmetric stretching

Table 35 Experimental and calculated vibrational frequencies of HATN-2Me-1ReA for FT-IR and FT-Raman.

$\nu_{FT\text{-}R}$ /cm^{-1}	$\nu_{FT\text{-}IR}$ /cm^{-1}	ν_{Calc} /cm^{-1}	S/A	Assignment from GaussView
	1088	1072	A	In plane delocalised ring distortions with H-wag
	1219	1210	A	In plane delocalised ring distortions with H-wag
	1362	1349	A	In plane delocalised ring distortions, strong on phenazine 1 and 2 with H-wag
	1489	1482	A	In plane delocalised ring distortions, strong on phenazine 1 and 2 with H-wag
	1907	1934		Out of sync CO stretching
	2023	2017		In sync CO stretching
449		464		CO stretching, small in plane distortions in phenezine 1
1348		1344	S	In plane delocalised ring distortions with H-wag
1413		1379	A	In plane delocalised ring distortions, stronger on rings 2 and 3 with H-wag
1473		1469	A	Weak in plane delocalised ring distortions, more H-wag and Me(H)-wag
1520		1505	A	In plane delocalised ring distortions, stronger in pyrazine rings with H-wag Me(H) wag
1570		1549	A	Strong in plane localised ring distortions on rings 2 and 3 with minor H-wag

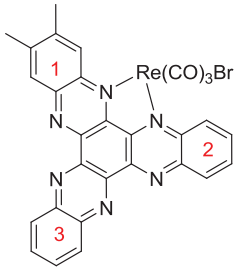

S/A indicates symmetric or asymmetric stretching

Table 36 Experimental and calculated vibrational frequencies of HATN-42Br-1ReS for FT-IR and FT-Raman.

$\nu_{FT\text{-}R}$ /cm^{-1}	$\nu_{FT\text{-}IR}$ /cm^{-1}	ν_{Calc} /cm^{-1}	S/A	Assignment from GaussView
	764	751	S	H-wag out of plane on ring 1 and 2
	1090	1069	S	In plane delocalised ring distortions with H-wag
	1358	1344	A	In plane delocalised ring distortions with H-wag
	1402	1393	S	In plane delocalised ring distortions with H-wag
	1439	1426	S	In plane delocalised ring distortions, strong on phenazine 3, with H-wag
	1489	1475	S	In plane delocalised ring distortions, stronger on rings 1 and 2 with H-wag
	1915	1937		Out of sync. CO stretching
	2025			In sync CO stretching
1334		1341	S	In plane delocalised ring distortions with H-wag
1419		1426	A	In plane delocalised ring distortions, stronger on ring 3 with H-wag
1518		1506	A	Strong pyrazine and central ring distortions with H-wag
1570		1546		In plane delocalised ring distortions, stronger on rings 1 and 2 with H-wag
2129		751		In sync CO stretching

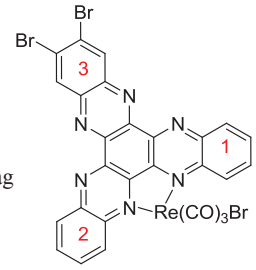

S/A indicates symmetric or asymmetric stretching

Table 37 Experimental and calculated vibrational frequencies of HATN-2Br-1ReA for FT-IR and FT-Raman.

$\nu_{FT\text{-}R}$ /cm^{-1}	$\nu_{FT\text{-}IR}$ /cm^{-1}	ν_{Calc} /cm^{-1}	S/A	Assignment from GaussView
	769	755	S	H-wag out of plane on ring 3
	1090	1078	A	In plane delocalised ring distortions, stronger on ring 2 with H-wag
	1358	1346	A	In plane delocalised ring distortions, strong on phenazine 3 with H-wag
	1400	1386	A	In plane delocalised ring distortions, strong on phenazine 1and 2 with H-wag
	1441	1432	A	In plane delocalised ring distortions, strong on phenazine 1 with H-wag
	1489	1480	A	In plane delocalised ring distortions, strong on phenazine 1 and 2 with H-wag
	1919	1966		Out of sync CO stretching
	2029	2053		In sync CO stretching
1358		1380		In plane delocalised ring distortions, strong on ring 3 with H-wag
1336		1340	S	In plane delocalised ring distortions with H-wag
1412		1421	A	In plane delocalised ring distortions, strong on phenazine 1 and 2 with H-wag
1516		1504	A	In plane delocalised ring distortions, strong on pyrazines with H-wag
1564		1547	A	In plane delocalised ring distortions, strong on phenazine 1 and 2 with H-wag
2125		2054		In sync CO stretching

S/A indicates symmetric or asymmetric stretching

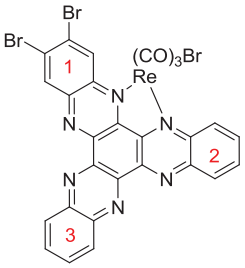

Table 38 Experimental and calculated vibrational frequencies of HATN-4Br2Me-1ReA for FT-IR.

$\nu_{FT\text{-}R}$ /cm^{-1}	$\nu_{FT\text{-}IR}$ /cm^{-1}	ν_{Calc} /cm^{-1}	S/A	Assignment from GaussView
	1099	1081	A	In plane delocalised ring distortions with H-wag
	1362	1378	S	In plane delocalised ring distortions, very strong on phenazine 2 and 3
	1446	1451	S	In plane delocalised ring distortions, strong on phenazine 1 and 2 with H-wag Me(H) wag
	1917	1938		Out of sync CO stretching
	2023	2023		In sync CO stretching

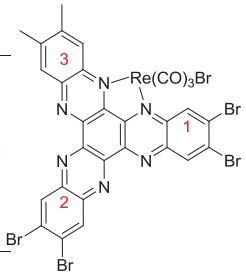

S/A indicates symmetric or asymmetric stretching

Table 39 Experimental and calculated vibrational frequencies of HATN-4Me2Br-2ReA for FT-IR.

ν_{FT-R} /cm^{-1}	ν_{FT-IR} /cm^{-1}	ν_{Calc} /cm^{-1}	S/A	Assignment from GaussView
	1105	2	A	In plane delocalised ring distortions, strong on phenazine 1 and 2 with H-wag
	1362	1346	S	In plane delocalised ring distortions, strong on phenazine 3 with H-wag
	1443	1449	S	In plane delocalised ring distortions, strong on phenazine 3 with H-wag
	1481	1477	A	In plane delocalised ring distortions, mainly H-wag and Me(H) wag
	1911	1936		Out of sync CO stretching
	2019	2022		In sync CO stretching

S/A indicates symmetric or asymmetric stretching

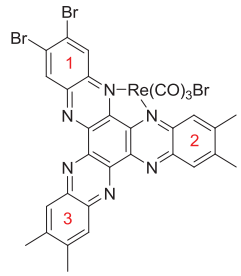

Table 40 Experimental and calculated vibrational frequencies of HATN-4Me2Br-1ReS for FT-IR and FT-Raman.

$\nu_{FT\text{-}R}$ /cm^{-1}	$\nu_{FT\text{-}IR}$ /cm^{-1}	ν_{Calc} /cm^{-1}	S/A	Assignment from GaussView
	1097	991		
	1360	1345	A	In plane delocalised ring distortions, strong on phenazine 1 and 2 with H-wag
	1441	1424	S	In plane delocalised ring distortions, strong on phenazine 3 with small Me(H) wag
	1483	1477	A	In plane delocalised ring distortions, mainly H-wag and Me(H) wag
	1903	1933		Out of sync CO stretching
	2021	2019		In sync CO stretching
1350		1350	S	Very strong in plane distortions in central ring with minor H-wag
1404		1377	A	In plane delocalised ring distortions, strong on phenazine 3
1467		1464	S	In plane delocalised ring distortions, strong on phenazine 1 and 2 with H-wag
1510		1502	A	In plane delocalised ring distortions, strong pyrazine distortions with H-wag
1566		1538	A	In plane delocalised ring distortions, strong on phenazine 1 and 2 with H-wag
2029		2019	S	In sync CO stretching

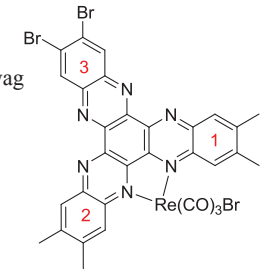

S/A indicates symmetric or asymmetric stretching

D.10 Copper Supplementary Information

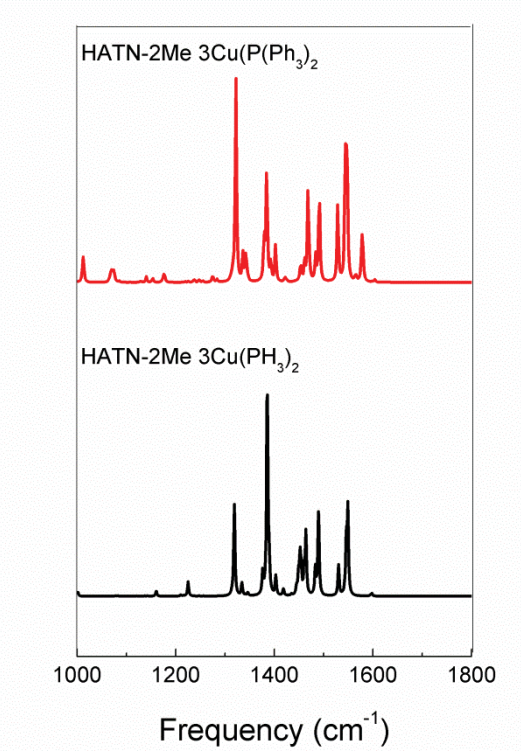

Figure 3 Comparison between HATN-2Me-3{Cu(P(Ph$_3$)$_2$} and HATN-2Me-3{Cu(PH$_3$)$_2$}.

D. 11 MAD values for copper-tetrafluoroborate complexes

Table 41 MAD values for copper complex experimental and calculated IR and FT-R data.

Complex	MAD value FT-IR	MAD value FT-R
HATN-4Me-3CuBF$_4$	18	14
HATN-2Me-3CuBF$_4$	32	16
HATN-2Br-3CuBF$_4$	14	15
HATN-4Br2Me-3CuBF$_4$	18	9
HATN-4Me2Br-3CuBF$_4$	9	8
HATN-4Br-3CuBF$_4$	24	12

D.12 UV-Vis data for HATN-3CuBF$_4$ complexes in acetonitrile

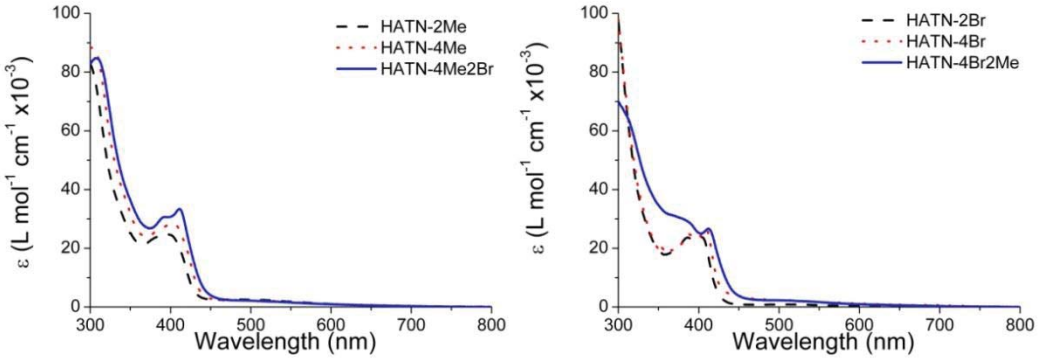

Table 42 λ_{max} and absorption coefficients of selected HATN-3CuBF$_4$ complexes.

HATN	λ (nm) / nm (ε / 10^3 L mol^{-1}cm^{-1})
HATN-2Me-3CuBF$_4$	386 (24.0), 398 (24.7), 450-599 (2.6-1.0)
HATN-4Me-3CuBF$_4$	390 (27.0), 403 (28.6), 450-601 (2.9-1.0)
HATN-4Me2Br-3CuBF$_4$	392 (30.7), 411 (33.4), 450-593 (2.5-1.0)
HATN-2Br-3CuBF$_4$	387 (23.7), 405 (23.7), 450 (0.9)
HATN-4Br-3CuBF$_4$	389 (24.6), 409 (27.0), 450-616 (3.8-1.0)
HATN-4Br2Me-3CuBF$_4$	385 (29.4), 412 (26.7), 450-595 (3.8-1.0)
HATN-4Me-3CuClO$_4$	386 (19.2), 404 (20.5), 450-661 (2.2-1.0)

D.13 FT-IR spectra for copper-tetrafluoroborate complexes

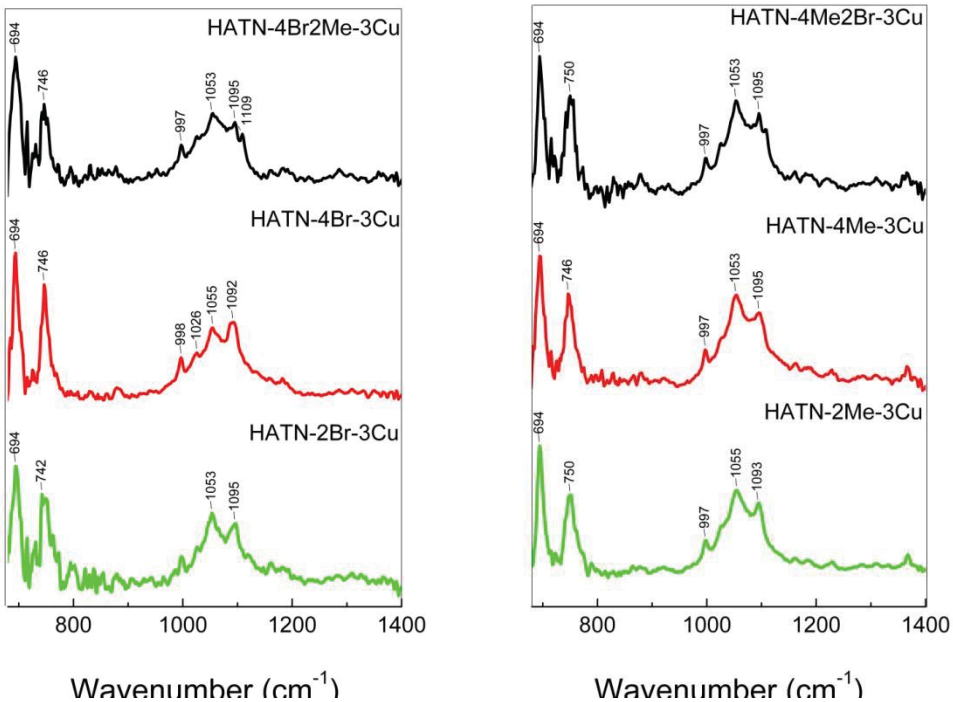

Figure 4 FT-IR spectra of HATN-3Cu compounds.

D.14 FT-Raman spectra for HATN-3CuBF$_4$ complexes

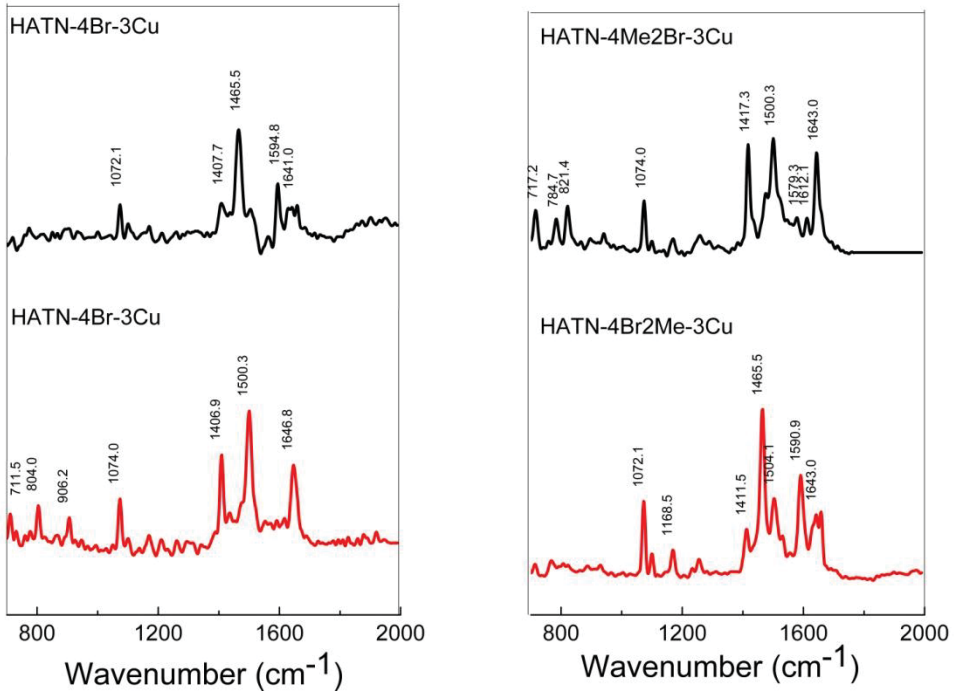

Figure 5 Raman spectra for HATN-3CuBF$_4$ complexes

D.15 Excitation tables for HATN-3CuBF4 complexes

Table 43 Summary of the first ten transitions calculated for the complex HATN-4Me-3CuBF$_4$ in CHCl$_3$. Only transitions with nonzero oscillator strengths are shown.

λ (nm)	E (eV)	*F*	Transition	Coefficients	Major Contributors	Assignment
745.20	1.6638	0.0600	HOMO-8 → LUMO+2	0.16944	Cu→π	MLCT
			HOMO-7 → LUMO	0.37648	Cu→π	
			HOMO-5 → LUMO	0.27879	Cu→π	
			HOMO→ LUMO	0.44650	Cu→π	
738.52	1.6788	0.0454	HOMO-8 → LUMO	0.12865	Cu→π	MLCT
			HOMO-8 → LUMO+1	-0.13090	Cu→π	
			HOMO-7 → LUMO+2	0.12451	Cu→π	
			HOMO-6 → LUMO	0.29170	Cu→π	
			HOMO-6 → LUMO+1	0.13959	Cu→π	
			HOMO-5 → LUMO	-0.10985	Cu→π	
			HOMO-4 → LUMO	0.30104	Cu→π	
			HOMO-1 → LUMO	0.44865	Cu→π	

Continued transitions for **HATN-4Me-3CuBF$_4$** in $CHCl_3$

λ (nm)	E (eV)	*F*	Transition	Coefficients	Major Contributors	Assignment
710.12	1.7460	0.0162	HOMO-8→ LUMO	0.46149	Cu→π	MLCT
			HOMO-7 → LUMO+2	0.19116	Cu→π	
			HOMO-6 → LUMO+1	-0.12969	Cu→π	
			HOMO-5→ LUMO+2	0.14640	Cu→π	
			HOMO-4 → LUMO	0.14918	Cu→π	
			HOMO-4 → LUMO+1	-0.14924	Cu→π	
			HOMO-3 → LUMO	0.27386	Cu→π	
			HOMO-2 → LUMO	-0.12994	Cu→π	
			HOMO-1 → LUMO	-0.21508	Cu→π	
705.66	1.7570	0.1094	HOMO-8 → LUMO+2	-0.13431	Cu→π	MLCT
			HOMO-7 → LUMO	-0.30426	Cu→π	
			HOMO-5 → LUMO	-0.25417	Cu→π	
			HOMO-4 → LUMO	-0.11790	Cu→π	
			HOMO-1 → LUMO	0.15626	Cu→π	
			HOMO → LUMO	0.50780	Cu→π	
701.61	1.7671	0.0557	HOMO-6 → LUMO	-0.21679	Cu→π	MLCT
			HOMO-6 → LUMO+1	-0.18102	Cu→π	
			HOMO-5 → LUMO	0.20442	Cu→π	
			HOMO-4→ LUMO	-0.23485	Cu→π	
			HOMO-4 → LUMO+1	-0.13210	Cu→π	
			HOMO-3 → LUMO	0.19995	Cu→π	
			HOMO-1 → LUMO	0.45621	Cu→π	
			HOMO → LUMO	-0.12824	Cu→π	

Continued transitions for **HATN-4Me-3CuBF$_4$** in $CHCl_3$

λ (nm)	E (eV)	*f*	Transition	Coefficients	Major Contributors	Assignment
694.01	1.7865	0.0204	HOMO-8 → LUMO	-0.30259	Cu→π	MLCT
			HOMO-7→ LUMO+2	-0.13357	Cu→π	
			HOMO-6 → LUMO+1	0.15673	Cu→π	
			HOMO-5 → LUMO+1	-0.12236	Cu→π	
			HOMO-4 → LUMO	0.21527	Cu→π	
			HOMO-4→ LUMO+2	-0.14119	Cu→π	
			HOMO-3 → LUMO	0.47781	Cu→π	
666.19	1.8611	0.0013	HOMO-7 → LUMO	-0.29333	Cu→π	MLCT
			HOMO-6 → LUMO	-0.22577	Cu→π	
			HOMO-6 → LUMO+1	-0.10606	Cu→π	
			HOMO-5 → LUMO	0.25850	Cu→π	
			HOMO-5 → LUMO+1	0.11028	Cu→π	
			HOMO-4 → LUMO	0.30333	Cu→π	
			HOMO-3 → LUMO	-0.17704	Cu→π	
			HOMO-3→ LUMO+1	-0.29918	Cu→π	
627.08	1.9772	0.0436	HOMO-8 → LUMO	0.12217	Cu→π	MLCT
			HOMO-2 → LUMO	0.63685	Cu→π	
			HOMO-1 → LUMO+1	-0.20790	Cu→π	
			HOMO → LUMO+2	-0.15130	Cu→π	
624.95	1.9839	0.1321	HOMO-2 → LUMO	0.23327	Cu→π	MLCT
			HOMO-1 → LUMO+1	0.57116	Cu→π	
			HOMO → LUMO+1	-0.14688	Cu→π	
			HOMO → LUMO+2	0.24920	Cu→π	

Continued transitions for **HATN-4Me-3CuBF$_4$** in $CHCl_3$

λ (nm)	E (eV)	*f*	Transition	Coefficients	Major Contributors	Assignment
620.79	1.9972	0.1339	HOMO-1 → LUMO+1	-0.11157	Cu→π	MLCT
			HOMO-1 → LUMO+2	0.51541	Cu→π	
			HOMO → LUMO+1	-0.42987	Cu→π	
			HOMO → LUMO+2	-0.14530	Cu→π	

Table 44 Summary of the first ten transitions calculated for the complex HATN-4Br-3CuBF$_4$ in CHCl$_3$. Only transitions with nonzero oscillator strengths are shown.

λ (nm)	E (eV)	*f*	Transition	Coefficients	Major Contributors	Assignment
817.35	1.5169	0.1397	HOMO-9 → LUMO	0.10728	Cu→π	MLCT
			HOMO-8 → LUMO	0.21034	Cu→π	
			HOMO-4 → LUMO	0.10613	Cu→π	
			HOMO → LUMO	0.63787	Cu→π	
811.29	1.5282	0.0794	HOMO-7 → LUMO	0.17180	Cu→π	MLCT
			HOMO-1 → LUMO	0.66071	Cu→π	
773.83	1.6022	0.0335	HOMO-9 → LUMO	0.23880	Cu→π	MLCT
			HOMO-9 → LUMO+2	-0.16269	Cu→π	
			HOMO-8 → LUMO	0.37964	Cu→π	
			HOMO-6→ LUMO	-0.24684	Cu→π	
			HOMO-4 → LUMO	0.26202	Cu→π	
			HOMO-3 → LUMO	-0.12980	Cu→π	
			HOMO → LUMO	-0.27545	Cu→π	
765.63	1.6194	0.0103	HOMO-9 → LUMO+1	-0.12625	Cu→π	MLCT
			HOMO-8→ LUMO	-0.14755	Cu→π	
			HOMO-8 → LUMO+1	0.17138	Cu→π	
			HOMO-7 → LUMO	0.38155	Cu→π	
			HOMO-7 → LUMO+2	0.16006	Cu→π	
			HOMO-6 → LUMO	-0.29795	Cu→π	
			HOMO-4 → LUMO	-0.17705	Cu→π	
			HOMO-3 → LUMO	-0.19019	Cu→π	
			HOMO-1 → LUMO	-0.20323	Cu→π	

Continued transitions for **HATN-4Br-3CuBF$_4$** in $CHCl_3$

λ (nm)	E (eV)	*f*	Transition	Coefficients	Major Contributors	Assignment
756.14	1.6397	0.0109	HOMO-9 → LUMO	-0.29345	Cu→π	MLCT
			HOMO-8 → LUMO	0.19154	Cu→π	
			HOMO-8 → LUMO+1	0.11916	Cu→π	
			HOMO-8 → LUMO+2	0.12442	Cu→π	
			HOMO-7 → LUMO	0.21180	Cu→π	
			HOMO-7 → LUMO+1	0.19346	Cu→π	
			HOMO-6 → LUMO+2	-0.12582	Cu→π	
			HOMO-4 → LUMO+1	-0.12424	Cu→π	
			HOMO-3 → LUMO	0.39763	Cu→π	
745.86	1.6623	0.0172	HOMO-9 → LUMO	0.40582	Cu→π	MLCT
			HOMO-8→ LUMO+2	-0.17268	Cu→π	
			HOMO-7 → LUMO	0.11014	Cu→π	
			HOMO-7 → LUMO+1	-0.19452	Cu→π	
			HOMO-6→ LUMO+2	-0.11517	Cu→π	
			HOMO-3→ LUMO	0.36206	Cu→π	
			HOMO-2→ LUMO	0.19770	Cu→π	
727.53	1.7042	0.0072	HOMO-1 → LUMO+2	-0.32552	Cu→π	MLCT
			HOMO → LUMO+1	0.59854	Cu→π	

Continued transitions for **HATN-4Br-3CuBF$_4$** in $CHCl_3$

λ (nm)	E (eV)	*f*	Transition	Coefficients	Major Contributors	Assignment
724.59	1.7111	0.0012	HOMO-8 → LUMO	0.21490	Cu→π	MLCT
			HOMO-7 → LUMO	0.23799	Cu→π	
			HOMO-6→ LUMO	0.44598	Cu→π	
			HOMO-4→ LUMO+1	0.19369	Cu→π	
			HOMO-3→ LUMO	-0.16382	Cu→π	
			HOMO-3→ LUMO+2	-0.18725	Cu→π	
			HOMO → LUMO+1	0.11908	Cu→π	
718.35	1.7260	0.0011	HOMO-8 → LUMO	-0.24398	Cu→π	MLCT
			HOMO-7 → LUMO	0.18546	Cu→π	
			HOMO-6→ 625	0.13902	Cu→π	
			HOMO-4→ LUMO	0.46535	Cu→π	
			HOMO-4→ LUMO+2	0.14967	Cu→π	
			HOMO-3→ LUMO+1	-0.26680	Cu→π	
694.20	1.7860	0.0369	HOMO-2→ LUMO	0.52028	Cu→π	MLCT
			HOMO-1→ LUMO+1	0.45279	Cu→π	

Table 45 Summary of the first ten transitions calculated for the complex HATN-2Me-3CuBF$_4$ in CHCl$_3$. Only transitions with nonzero oscillator strengths are shown.

λ (nm)	E (eV)	*f*	Transition	Coefficients	Major Contributors	Assignment
760.56	1.6302	0.0686	HOMO-8 → LUMO	0.15119	Cu→π	MLCT
			HOMO-8 → LUMO+2	-0.15974	Cu→π	
			HOMO-7 → LUMO	0.35475	Cu→π	
			HOMO-5 → LUMO	0.18936	Cu→π	
			HOMO-4→ LUMO	0.18638	Cu→π	
			HOMO → LUMO	0.45687	Cu→π	
752.63	1.6473	0.0626	HOMO-8 → LUMO+1	0.11920	Cu→π	MLCT
			HOMO-7 → LUMO+1	-0.13561	Cu→π	
			HOMO-6 → LUMO	0.30724	Cu→π	
			HOMO-6 → LUMO+2	0.10916	Cu→π	
			HOMO-5 → LUMO	-0.19464	Cu→π	
			HOMO-4 → LUMO	0.17213	Cu→π	
			HOMO-1 → LUMO	0.49651	Cu→π	
			HOMO → LUMO	-0.12764	Cu→π	
723.60	1.7134	0.0661	HOMO-8 → LUMO	0.38402	Cu→π	MLCT
			HOMO-7 → LUMO	0.12447	Cu→π	
			HOMO-7 → LUMO+2	-0.15302	Cu→π	
			HOMO-5 → LUMO	0.18941	Cu→π	
			HOMO-5 → LUMO+2	-0.10772	Cu→π	
			HOMO-4 → LUMO	0.12161	Cu→π	
			HOMO-3 → LUMO	0.20372	Cu→π	
			HOMO-1 → LUMO	-0.11149	Cu→π	
			HOMO → LUMO	-0.38257	Cu→π	

Continued transitions for **HATN-2Me-3CuBF$_4$** in $CHCl_3$

λ (nm)	E (eV)	*f*	Transition	Coefficients	Major Contributors	Assignment
718.65	1.7252	0.0587	HOMO-7 → LUMO	-0.18953	Cu→π	MLCT
			HOMO-6 → LUMO	-0.22531	Cu→π	
			HOMO-6 → LUMO+1	0.13231	Cu→π	
			HOMO-5 → LUMO	0.21204	Cu→π	
			HOMO-4 → LUMO	-0.24742	Cu→π	
			HOMO-4 → LUMO+1	0.10320	Cu→π	
			HOMO-3 → LUMO	0.18121	Cu→π	
			HOMO-1 → LUMO	0.42881	Cu→π	
716.44	1.7306	0.0489	HOMO-8→ LUMO	0.23758	Cu→π	MLCT
			HOMO-7 → LUMO	-0.23969	Cu→π	
			HOMO-7 → LUMO+1	-0.12576	Cu→π	
			HOMO-6 → LUMO	0.15811	Cu→π	
			HOMO-6 → LUMO+1	0.15927	Cu→π	
			HOMO-5 → LUMO	-0.23260	Cu→π	
			HOMO-3 → LUMO	0.21588	Cu→π	
			HOMO-1 → LUMO	-0.17933	Cu→π	
			HOMO → LUMO	0.33122	Cu→π	

Continued transitions for **HATN-2Me-3CuBF$_4$** in $CHCl_3$

λ (nm)	E (eV)	*f*	Transition	Coefficients	Major Contributors	Assignment
706.95	1.7538	0.0208	HOMO-8 → LUMO	-0.30883	Cu→π	MLCT
			HOMO-7 → LUMO+2	0.13599	Cu→π	
			HOMO-6 → LUMO	0.13499	Cu→π	
			HOMO-6 → LUMO+1	-0.16523	Cu→π	
			HOMO-5 → LUMO	0.12817	Cu→π	
			HOMO-5 → LUMO+2	-0.14754	Cu→π	
			HOMO-3 → LUMO	0.48510	Cu→π	
683.43	1.8141	0.0015	HOMO-7 → LUMO	-0.26352	Cu→π	MLCT
			HOMO-6 → LUMO	0.29282	Cu→π	
			HOMO-5 → LUMO	0.40514	Cu→π	
			HOMO-5 → LUMO+2	-0.10584	Cu→π	
			HOMO-4 → LUMO+1	-0.18311	Cu→π	
			HOMO-3 → LUMO	-0.17082	Cu→π	
			HOMO-3 → LUMO+2	-0.19808	Cu→π	
665.42	1.8632	0.0018	HOMO-1 → LUMO+1	0.17076	Cu→π	MLCT
			HOMO-1 → LUMO+2	0.37950	Cu→π	
			HOMO → LUMO+1	0.54234	Cu→π	
			HOMO → LUMO+2	-0.14129	Cu→π	
638.45	1.9420	0.0673	HOMO-2 → LUMO	0.51864	Cu→π	MLCT
			HOMO-1 → LUMO+1	-0.42671	Cu→π	
			HOMO → LUMO+1	0.13540	Cu→π	

Continued transitions for **HATN-2Me-3CuBF$_4$** in $CHCl_3$

λ (nm)	E (eV)	*f*	Transition	Coefficients	Major Contributors	Assignment
636.65	1.9474	0.1824	HOMO-1 → LUMO+1	-0.16412	Cu→π	MLCT
			HOMO-1 → LUMO+2	0.51924	Cu→π	
			HOMO → LUMO+1	-0.36892	Cu→π	
			HOMO → LUMO+2	-0.22752	Cu→π	

Table 46 Summary of the first ten transitions calculated for the complex HATN-4Br2Me-3CuBF$_4$ in CHCl$_3$. Only transitions with nonzero oscillator strengths are shown.

λ (nm)	E (eV)	*f*	Transition	Coefficients	Major Contributors	Assignment
809.19	1.5322	0.1361	HOMO-8 → LUMO	0.17860	Cu→π*	MLCT
			HOMO-7 → LUMO	-0.20305	Cu→π*	
			HOMO-4 → LUMO	-0.10398	Cu→π*	
			HOMO → LUMO	0.61900	Cu→π*	
800.70	1.5484	0.0582	HOMO-6 → LUMO	0.16103	Cu→π*	MLCT
			HOMO-1 → LUMO	0.65792	Cu→π*	
767.48	1.6155	0.0445	HOMO-8 → LUMO	0.35127	Cu→π*	MLCT
			HOMO-8 → LUMO+2	-0.14024	Cu→π*	
			HOMO-7 → LUMO	-0.28022	Cu→π*	
			HOMO-5 → LUMO	-0.32561	Cu→π*	
			HOMO-4 → LUMO	-0.17474	Cu→π*	
			HOMO-3→ LUMO	-0.11466	Cu→π*	
			HOMO → LUMO	-0.30886	Cu→π*	
755.57	1.6409	0.0109	HOMO-7 → LUMO	-0.16893	Cu→π*	MLCT
			HOMO-7 → LUMO+1	0.18693	Cu→π*	
			HOMO-6 → LUMO	-0.31396	Cu→π*	
			HOMO-6 → LUMO+2	-0.14749	Cu→π*	
			HOMO-5 → LUMO	0.32057	Cu→π*	
			HOMO-4 → LUMO	-0.24998	Cu→π*	
			HOMO-4 → LUMO+1	0.10648	Cu→π*	
			HOMO-3 → LUMO	0.18536	Cu→π*	
			HOMO-1 → LUMO	0.20003	Cu→π*	

Continued transitions for **HATN-4Br2Me-3CuBF$_4$** in $CHCl_3$

λ (nm)	E (eV)	*f*	Transition	Coefficients	Major Contributors	Assignment
745.99	1.6620	0.0073	HOMO-8 → LUMO	-0.24582	Cu→π*	MLCT
			HOMO-7 → LUMO	-0.26607	Cu→π*	
			HOMO-7 → LUMO+1	-0.13817	Cu→π*	
			HOMO-7 → LUMO+2	-0.13509	Cu→π*	
			HOMO-6 → LUMO	0.21440	Cu→π*	
			HOMO-6 → LUMO+1	0.21143	Cu→π*	
			HOMO-5 → LUMO+2	-0.10947	Cu→π*	
			HOMO-4 → LUMO+1	0.13911	Cu→π*	
			HOMO-3 → LUMO	0.35802	Cu→π*	
			HOMO-2 → LUMO	-0.10953	Cu→π*	
737.31	1.6816	0.0149	HOMO-8 → LUMO	0.36147	Cu→π*	MLCT
			HOMO-7 → LUMO+2	0.14021	Cu→π*	
			HOMO-6 → LUMO	0.19069	Cu→π*	
			HOMO-6 → LUMO+1	-0.18947	Cu→π*	
			HOMO-5 → LUMO	0.16804	Cu→π*	
			HOMO-5 → LUMO+2	-0.10201	Cu→π*	
			HOMO-4 → LUMO	0.10353	Cu→π*	
			HOMO-3 → LUMO	0.34193	Cu→π*	
			HOMO-2 → LUMO	0.20651	Cu→π*	

Continued transitions for **HATN-4Br2Me-3CuBF$_4$** in $CHCl_3$

λ (nm)	E (eV)	*f*	Transition	Coefficients	Major Contributors	Assignment
			HOMO-7 → LUMO	-0.20485	Cu→π*	
			HOMO-6 → LUMO	0.26768	Cu→π*	
			HOMO-5 → LUMO	0.37422	Cu→π*	
714.73	1.7347	0.0042	HOMO-4 → LUMO+1	-0.21465	Cu→π*	MLCT
			HOMO-3 → LUMO	-0.27577	Cu→π*	
			HOMO-3 → LUMO+2	-0.16589	Cu→π*	
			HOMO → LUMO+1	-0.13655	Cu→π*	
			HOMO-5 → LUMO	0.11211	Cu→π*	
713.24	1.7383	0.0255	HOMO-1 → LUMO+2	-0.21178	Cu→π*	MLCT
			HOMO → LUMO+1	0.64431	Cu→π*	
			HOMO-8 → LUMO	-0.14614	Cu→π*	
687.50	1.8034	0.0191	HOMO-2 → LUMO	0.61612	Cu→π*	MLCT
			HOMO-1 → LUMO+1	0.28251	Cu→π*	
			HOMO-8 → LUMO	0.12638	Cu→π*	
679.99	1.8233	0.0847	HOMO-2 → LUMO	-0.23490	Cu→π*	MLCT
			HOMO-1 → LUMO+1	0.62357	Cu→π*	

Table 47 Summary of the first ten transitions calculated for the complex HATN-2Br-3CuBF$_4$ in CHCl$_3$. Only transitions with nonzero oscillator strengths are shown.

λ (nm)	E (eV)	*f*	Transition	Coefficients	Major Contributors	Assignment
796.1	1.5574	0.1294	HOMO-8→ LUMO+2	-0.11552	Cu→π*	MLCT
			HOMO-7→ LUMO	0.28221	Cu→π*	
			HOMO-5 → LUMO	0.11373	Cu→π*	
			HOMO-4 → LUMO	0.12972	Cu→π*	
			HOMO-1 → LUMO	-0.15726	Cu→π*	
			HOMO → LUMO	0.57369	Cu→π*	
787.95	1.5735	0.0721	HOMO-8 → LUMO	-0.11898	Cu→π*	MLCT
			HOMO-6 → LUMO	0.21523	Cu→π*	
			HOMO-1 → LUMO	0.59543	Cu→π*	
			HOMO → LUMO	0.17757	Cu→π*	
756.02	1.6399	0.0588	HOMO-8 → LUMO+2	-0.17293		MLCT
			HOMO-7 → LUMO	0.42877	Cu→π*	
			HOMO-5 → LUMO	0.26896	Cu→π*	
			HOMO-4 → LUMO	0.19296	Cu→π*	
			HOMO → LUMO	-0.35663		

Continued transitions for **HATN-2Br-3CuBF$_4$** in $CHCl_3$

λ (nm)	E (eV)	*f*	Transition	Coefficients	Major Contributors	Assignment
750.12	1.6529	0.0201	HOMO-8 → LUMO	0.28230	Cu→π*	MLCT
			HOMO-8 → LUMO+1	-0.11523	Cu→π*	
			HOMO-7→ LUMO+2	-0.18093	Cu→π*	
			HOMO-6 → LUMO	-0.29850	Cu→π*	
			HOMO-6 → LUMO+1	-0.11735	Cu→π*	
			HOMO-5 → LUMO	-0.17548	Cu→π*	
			HOMO-5→ LUMO+2	-0.10747	Cu→π*	
			HOMO-4 → LUMO	0.28981	Cu→π*	
			HOMO-3 → LUMO	0.15542	Cu→π*	
			HOMO-1 → LUMO	0.31230	Cu→π*	
742.74	1.6693	0.0080	HOMO-8 → LUMO	0.31321	Cu→π*	MLCT
			HOMO-7→ LUMO	-0.12439	Cu→π*	
			HOMO-6 → LUMO	0.21858	Cu→π*	
			HOMO-6→ LUMO+1	0.28311	Cu→π*	
			HOMO-5 → LUMO	0.16769	Cu→π*	
			HOMO-5→ LUMO+2	-0.11390	Cu→π*	
			HOMO-4 → LUMO+1	-0.15434	Cu→π*	
			HOMO-3 → LUMO	0.34428	Cu→π*	
			HOMO-2 → LUMO	0.10449	Cu→π*	
			HOMO-1 → LUMO+1	0.10033	Cu→π*	

Continued transitions for **HATN-2Br-3CuBF$_4$** in $CHCl_3$

λ (nm)	E (eV)	*f*	Transition	Coefficients	Major Contributors	Assignment
732.42	1.6928	0.0208	HOMO-8→ LUMO	-0.36667	Cu→π*	MLCT
			HOMO-7 → LUMO+2	0.15991	Cu→π*	
			HOMO-6 → LUMO+1	-0.15758	Cu→π*	
			HOMO-5→ LUMO+2	-0.10221	Cu→π*	
			HOMO-4→ LUMO	0.19231	Cu→π*	
			HOMO-3 → LUMO	0.42709	Cu→π*	
			HOMO-2 → LUMO	-0.13407	Cu→π*	
704.47	1.7600	0.0011	HOMO-7 → LUMO	-0.28708	Cu→π*	MLCT
			HOMO-6→ LUMO	0.10621	Cu→π*	
			HOMO-5 → LUMO	0.17884	Cu→π*	
			HOMO-5 → LUMO+2	-0.10316	Cu→π*	
			HOMO-4 → LUMO	0.38677	Cu→π*	
			HOMO-4 → LUMO+1	0.13350	Cu→π*	
			HOMO-3 → LUMO	-0.19026	Cu→π*	
			HOMO-3 → LUMO+1	-0.30657	Cu→π*	
700.11	1.7709	0.0027	HOMO-1 → LUMO+1	-0.11283	Cu→π*	MLCT
			HOMO-1 → LUMO+2	0.41952	Cu→π*	
			HOMO → LUMO+1	0.52396	Cu→π*	
			HOMO → LUMO+2	0.10500	Cu→π*	
672.65	1.8432	0.1149	HOMO-2 → LUMO	-0.42939	Cu→π*	MLCT
			HOMO-1 → LUMO+1	0.50117	Cu→π*	
			HOMO → LUMO+2	0.20044	Cu→π*	

Continued transitions for **HATN-2Br-3CuBF$_4$** in $CHCl_3$

λ (nm)	E (eV)	*f*	Transition	Coefficients	Major Contributors	Assignment
670.70	1.8486	0.1117	HOMO-8→ LUMO	-0.10737	Cu→π*	MLCT
			HOMO-2 → LUMO	0.51152	Cu→π*	
			HOMO-1 → LUMO+1	0.29968	Cu→π*	
			HOMO → LUMO+2	0.33457	Cu→π*	

Table 48 Summary of the first ten transitions calculated for the complex HATN-4Me2Br-3CuBF$_4$ in CHCl$_3$. Only transitions with nonzero oscillator strengths are shown.

λ (nm)	E (eV)	*f*	Transition	Coefficients	Major Contributors	Assignment
778.11	1.5934	0.1059	HOMO-8 → LUMO+2	-0.12753	Cu→π*	MLCT
			HOMO-7 → LUMO	0.32135	Cu→π*	
			HOMO-5 → LUMO	0.17853	Cu→π*	
			HOMO-4 → LUMO	0.13801	Cu→π*	
			HOMO → LUMO	0.55282	Cu→π*	
761.51	1.6281	0.0378	HOMO-8 → LUMO	-0.22073	Cu→π*	MLCT
			HOMO-7 → LUMO+2	0.11347	Cu→π*	
			HOMO-6 → LUMO	0.16661	Cu→π*	
			HOMO-5→ LUMO	0.11127	Cu→π*	
			HOMO-4 → LUMO	-0.14961	Cu→π*	
			HOMO-1 → LUMO	0.58411	Cu→π*	
737.45	1.6813	0.0838	HOMO-8 → LUMO+2	0.15499	Cu→π*	MLCT
			HOMO-7 → LUMO	-0.39566	Cu→π*	
			HOMO-5 → LUMO	-0.29819	Cu→π*	
			HOMO-4 → LUMO	-0.16102	Cu→π*	
			HOMO → LUMO	0.41903	Cu→π*	
731.72	1.6944	0.0152	HOMO-8 → LUMO	0.39843	Cu→π*	MLCT
			HOMO-7 → LUMO+2	-0.17571	Cu→π*	
			HOMO-5 → LUMO+2	-0.11993	Cu→π*	
			HOMO-4 → LUMO	0.30602	Cu→π*	
			HOMO-3 → LUMO	0.19318	Cu→π*	
			HOMO-1 → LUMO	0.33967	Cu→π*	

Continued transitions for **HATN-4Me2Br-3CuBF$_4$** in $CHCl_3$

λ (nm)	E (eV)	*f*	Transition	Coefficients	Major Contributors	Assignment
716.73	1.7299	0.0092	HOMO-7 → LUMO	-0.16474	Cu→π*	MLCT
			HOMO-6 → LUMO	0.21626	Cu→π*	
			HOMO-6 → LUMO+1	0.24289	Cu→π*	
			HOMO-5 → LUMO	0.29491	Cu→π*	
			HOMO-5 → LUMO+2	-0.10435	Cu→π*	
			HOMO-4 → LUMO+1	-0.17743	Cu→π*	
			HOMO-3 → LUMO	0.36778	Cu→π*	
			HOMO-3 → LUMO+1	0.12076	Cu→π*	
			HOMO-1 → LUMO	-0.17558	Cu→π*	
			HOMO-1 → LUMO+1	0.10734	Cu→π*	
713.10	1.7387	0.0119	HOMO-8 → LUMO	0.36506	Cu→π*	MLCT
			HOMO-7 → LUMO+2	-0.12622	Cu→π*	
			HOMO-6 → LUMO+1	0.21372	Cu→π*	
			HOMO-5 → LUMO+1	0.10208	Cu→π*	
			HOMO-4 → LUMO	-0.34447	Cu→π*	
			HOMO-4 → LUMO+2	-0.12619	Cu→π*	
			HOMO-3 → LUMO	-0.28695	Cu→π*	
			HOMO-2 → LUMO	0.17562	Cu→π*	

Continued transitions for **HATN-4Me2Br-3CuBF$_4$** in $CHCl_3$

λ (nm)	E (eV)	*f*	Transition	Coefficients	Major Contributors	Assignment
675.30	1.8360	0.0027	HOMO-7 → LUMO	0.23655	Cu→π*	MLCT
			HOMO-6 → LUMO	-0.18013	Cu→π*	
			HOMO-6 → LUMO+1	-0.12865	Cu→π*	
			HOMO-5 → LUMO	-0.17323	Cu→π*	
			HOMO-5 → LUMO+1	-0.11362	Cu→π*	
			HOMO-4 → LUMO	-0.28278	Cu→π*	
			HOMO-3 → LUMO	0.29400	Cu→π*	
			HOMO-3 → LUMO+1	0.36584	Cu→π*	
665.56	1.8628	0.0071	HOMO-1 → LUMO+2	0.43600	Cu→π*	MLCT
			HOMO → LUMO+1	0.53197	Cu→π*	
657.20	1.8866	0.0043	HOMO-8 → LUMO	-0.16466	Cu→π*	MLCT
			HOMO-2 → LUMO	0.66178	Cu→π*	
643.45	1.9269	0.2353	HOMO-6 → LUMO	-0.10463	Cu→π*	MLCT
			HOMO-1 → LUMO+1	0.60713	Cu→π*	
			HOMO → LUMO+2	0.30806	Cu→π*	

D.16 Experimental and calculated vibrational frequencies for HATN-3CuBF$_4$

Table 49 Experimental and calculated vibrational frequencies of HATN-4Me-3CuBF$_4$ for FT-IR and FT-Raman.

ν_{FT-R} /cm^{-1}	ν_{FT-IR} /cm^{-1}	ν_{Calc} /cm^{-1}	S/A	Assignment from GaussView
735		702	S	In plane delocalised ring distortions on HATN rings
1001		1010	S	Minor ring distortions on HATN and phenyl rings with H-wag
1361		1326	S	In plane delocalised ring distortions on HATN, stronger in central ring with H-wag
1400		1386	S	In plane delocalised ring distortions on HATN, stronger in methyl phenazines with H-wag
1477		1485	S	In plane delocalised ring distortions on HATN, stronger in non-functionalised phenazine with H-wag
1520		1521	S	In plane delocalised ring distortions on HATN with H-wag
1568		1544	S	In plane delocalised ring distortions on HATN stronger on non-functionalised phenazine with H-wag
	694	681		PPh_3 Phenyl distortions
	746	732		PPh_3 Phenyl distortions with out of plane H-wag
	997	992	S	(Me)H rocking with small distortions on the methyl rings
	1053	1088	S	In plane delocalised ring distortions with H-wag
	1095	1094	S	In plane delocalised ring distortions with H-wag

S/A indicates symmetric or asymmetric stretching

Table 50 Experimental and calculated vibrational frequencies of HATN-4Br-3CuBF$_4$ for FT-IR and FT-Raman.

ν_{FT-R} /cm^{-1}	ν_{FT-IR} /cm^{-1}	ν_{Calc} /cm^{-1}	S/A	Assignment from GaussView
1072		1068		Minor ring distortions on HATN and phenyl rings with H-wag
1448		1381	S	In plane delocalised ring distortions on HATN, stronger in central ring
1466		1427	A	In plane delocalised ring distortions on HATN, stronger in bromo phenzines with H-wag
1595		1578		
	694	678		Phosphine-Phenyl distortions with out of plane H-wag
	746	729		Phosphine-Phenyl distortions with out of plane H-wag
	998	975		Phosphine-Phenyl distortions with out of plane H-wag
	1026	1012		Phosphine-Phenyl distortions with out of plane H-wag
	1055	1072	S	Localised in plane distortions on Br phenazine with H-wag
	1092	1084	A	In plane delocalised ring distortions on HATN with H-wag

S/A indicates symmetric or asymmetric stretching

Table 51 Experimental and calculated vibrational frequencies of HATN-2Me-3CuBF$_4$ for FT-IR and FT-Raman.

ν_{FT-R} /cm^{-1}	ν_{FT-IR} /cm^{-1}	ν_{Calc} /cm^{-1}	S/A	Assignment from GaussView
717		708	S	In plane delocalised ring distortions on HATN rings
746		733	S	Minor ring distortions on HATN and phenyl rings with H-wag
798		782	S	In plane delocalised ring distortions on HATN with H-wag
852		839	S	In plane delocalised ring distortions on HATN, stronger in triphenylphosphine phenyl rings with H-wag
1001		1010	S	Minor ring distortions on tripheynylphosphine phenyl rings with H-wag
1338		1320	S	In plane delocalised ring distortions on HATN stronger on .non-functionalised phenazine
1479		1490	A	In plane delocalised ring distortions on HATN stronger on non-functionalised phenazine
1514		1546	A	In plane delocalised ring distortions on HATN stronger on non-functionalised phenazine
1577		1576		Minor ring distortions on tripheynylphosphine phenyl rings with H-wag
	694	683		Phosphine-Phenyl distortions with out of plane H-wag
	750	731		Phosphine-Phenyl distortions with out of plane H-wag
	997	993	S	Me(H) rocking with minor in plane Me ring distortions
	1055	1084	A	In plane delocalised ring distortions on HATN with H-wag
	1093	1079	S	In plane delocalised ring distortions on HATN with H-wag

S/A indicates symmetric or asymmetric stretching

Table 52 Experimental and calculated vibrational frequencies of HATN-2Br-3CuBF$_4$ for FT-IR and FT-Raman.

ν_{FT-R} /cm^{-1}	ν_{FT-IR} /cm^{-1}	ν_{Calc} /cm^{-1}	S/A	Assignment from GaussView
804.0		820	S	In plane delocalised ring distortions on HATN, small phenyl ring distortions
906.2		973		Phenyl ring distortions
1074.0		1073		Phenyl ring distortions
1406.9		1382	S	In plane delocalised ring distortions on HATN, stronger in central ring
1500.3		1489	A	In plane delocalised ring distortions on HATN, stronger in non-functionalised quinoxalines with H-wag
	694	680		Phosphine-Phenyl distortions with out of plane H-wag
	742	745		Phosphine-Phenyl distortions with out of plane H-wag
	1053	1068	A	HATN H-wag P-phenyl H-wag
	1095	1080	S	In plane delocalised ring distortions on HATN

S/A indicates symmetric or asymmetric stretching

Table 53 Experimental and calculated vibrational frequencies of HATN-4Br2Me-3CuBF$_4$ for FT-IR and FT-Raman.

ν_{FT-R} /cm^{-1}	ν_{FT-IR} /cm^{-1}	ν_{Calc} /cm^{-1}	S/A	Assignment from GaussView
1072.1		1118.02		Phenyl ring distortions
1165.8		1223.38		Phenyl ring distortions
1411.5		1442.96	A	In plane delocalised ring distortions on HATN
1465.5		1536.54	S	In plane localised ring distortions on HATN methyl ring, with H-wag
1504.1		1566.75	S	In plane delocalised ring distortions on HATN with H-wag
1590.9		1594.36	S	In plane delocalised ring distortions on HATN, stronger in methyl phenazine with H-wag
1643.0				
	694	708.75		Phosphine-Phenyl distortions with out of plane H-wag
	746	763.83		Phosphine-Phenyl distortions with out of plane H-wag with minor HATN distortions
	997	1034.04	S	Me(H) rocking with small in plane distortions in then Me rings
	1053	1117.26	A	Br ring distortion H-wag. Minor P-phenyl distortions
	1095	1136.86	A	Delocalised in plane distortions with H-wag
	1109	1152.42	A	Localised in plane distortions in Me phenazine

S/A indicates symmetric or asymmetric stretching

Table 54 Experimental and calculated vibrational frequencies of HATN-4Me2Br-3CuBF$_4$ for FT-IR and FT-Raman.

ν_{FT-R} /cm^{-1}	ν_{FT-IR} /cm^{-1}	ν_{Calc} /cm^{-1}	S/A	Assignment from GaussView
717		703	S	Delocalised in plane distortions with H-wag and Me(H) rocking
784		807	S	Delocalised in plane distortions with H-wag and Me(H) rocking
821		820	A	Delocalised in plane distortions with H-wag and Me(H) rocking
1074		1072		Phosphine-Phenyl distortions
1417		1425	S	Me(H) rocking with H wag and minor HATN in plane distortions
1500		1510	S	Me(H) rocking with H wag and minor HATN in plane distortions
1579		1578		Phosphine-Phenyl distortions
1612		1604		Delocalised in plane distortions with H-wag, stronger in bromo ring
	694	708.75		Phosphine-Phenyl distortions with out of plane H-wag
	746	763.83	S	Phosphine-Phenyl distortions with out of plane H-wag with minor HATN distortions
	997	1034.04	S	Me(H) rocking with small in plane distortions in then Me rings
	1053	117.26	A	HATN in plane ring distortions in bromo rings with H-wag, minor P-phenyl distortions
	1095	1136.86	A	Delocalised in plane distortions with H-wag
	1109	1152.42	A	HATN in plane ring distortions localised on methyl ring with H-wag

S/A indicates symmetric or asymmetric stretching

References

1 Skujins, S. W., G. *Tetrahedron* **1969**, *25*, 3935.
2 Paula, Q. A. d.; Batista, A. A.; Nascimento, O. R.; Costa-Filho, A. J. d.; Schultz, M. S.; Bonfadini, M. R.; Oliva, G. *Journal of the Brazilian Chemical Society* **2000**, *11*, 530.
3 Okawara, T.; Hashimoto, K.; Abe, M.; Shimakoshi, H.; Hisaeda, Y. *Chemical Communications* **2012**, *48*, 5413.
4 Kim, G.; Basarir, F.; Yoon, T.-H. *Synthetic Metals* **2011**, *161*, 2092.